Natural variation suggests new mechanisms for bract development inArabidopsis, desynchronising bract suppression from the floral transition

Sana Dieudonné, Ruth Kristianingsih, Stéphanie Laine, Béline Jesson, Véronique Vidal, Rachel Wells, Richard Morris, Fabrice Besnard

Running title : bract natural variation

Natural variation suggests new mechanisms for bract development in *Arabidopsis*, desynchronising bract suppression from the floral transition

Dieudonné Sana[1], Kristianingsih Ruth[3], Laine Stéphanie[1], Jesson Béline[2], Vidal Véronique[2], Wells Rachel[4], Morris Richard[3] and Besnard Fabrice[1]

[1]*Laboratoire RDP, (Univ. Lyon, ENS de Lyon, UCB Lyon 1, CNRS, INRAe, Inria), Lyon, France;* [2]*Helixio, Clermont-Ferrand, France;* [3]*Department of Computational and Systems Biology, John Innes Centre, Norwich, United Kingdom and* [4]*Department of Crop Genetics, John Innes Centre, Norwich, United Kingdom.*

correspondance: fabrice.besnard@ens-lyon.fr

Word count indication:

section	Word count
Introduction	1301
Materials and Methods	3316
Results	4003
Discussion	1465

This manuscript contains 6 main figures, 16 supporting figures and 8 supporting tables

Content

SUMMARY
Introduction
Materials and Methods
Results
Discussion
Acknowledgements
Competing interests,
Author contributions
Data availability
References
Supporting Information

Running title : bract natural variation

Figure legends

SUMMARY

- Bracts, the leaves subtending flowers, were lost multiple times in angiosperms, including in *Brassicaceae*, where their development is blocked early. *Arabidopsis* mutants that restore bract formation suggest that flower identity genes suppress the vegetative program of bract development, but the exact mechanisms and the evolutionary origin of bract loss remain unclear.
- We exploited natural variation in bracts that form only at the base of flowering branches in *Arabidopsis*, to study bract development and its connection to floral transition. We combined multiscale phenotyping, quantitative genetics, meristem imaging, time-series transcriptomics and curve registration to capture the genetic and developmental mechanisms unlocking bract development during floral transition.
- We mapped four Quantitative Trait Loci controlling bracts, excluding known bract mutant genes. We demonstrated LEAFY and other flower regulators were not involved and identified lists of new candidate genes and pathways, such as the anthocyanin pathway. We found that bract develops when gene expression is desynchronised from the floral transition, either later or earlier, revealing a more complex landscape than the previously proposed prolonged vegetative state.
- We identified new mechanisms unlocking bract development. This natural variation sheds a new light on development canalisation during floral transition and on bract loss evolution.

5–8 key words

Arabidopsis natural variation, bract, evolutionary loss, floral transition, heterochrony, quantitative genetics, time registration, time-series transcriptomics.

Introduction

Morphological evolution sometimes proceeds by losing structures or by regaining lost traits. The genetic and developmental mechanisms leading to a trait loss or regain are being elucidated (Cronk 2009; Sadier et al. 2022). Trait loss can simply result from gene(s) loss (Xu et al. 2019). However, pleiotropy (one gene having different functions) can limit gene loss if it causes detrimental effects and reduces fitness (Helsen et al. 2020). Also, a full genetic knock-out of a trait may hinder its regain (Sadier et al. 2022). Hence, more studies are needed to unravel the mechanisms behind the evolution of trait loss or regain.

In flowering plants, bracts provide an interesting model to address this loss and regain question as they have been repeatedly lost and sometimes regained in different groups. Bracts refer to any leaves developing in the inflorescence of angiosperms such as the edible leaves of an artichoke. More accurately in botany, bracts are the leaves subtending a single flower, at the junction of the floral peduncle with the stem (Dinneny et al. 2004; Endress 2006; Prenner et al. 2009). Bracts have evolved a wide diversity aligned to various adaptive functions: photosynthesis, mechanical protection, pollinator attraction or seed dispersion. Some of these adaptive changes have resulted in bract reduction or loss, like in *Poaceae* (grasses) or *Brassicaceae* (cabbages). This loss may be an evolutionary adaptation to specific pollinators or anemogamy, privileged resource allocation into reproductive versus vegetative organs or developmental constraints (Whipple et al. 2010). To investigate the underlying genetic and developmental mechanisms, several studies have been led in *Poaceae* (using rice, maize, wheat and barley) and in *Arabidopsis thaliana* for *Brassicaceae*.

In these two groups, the reduced bracts are not strictly homologous. In *Poaceae* inflorescences (ear, panicles or tassels), bracts are suppressed at major branching points while the bracts closely associated with the floral unit (florets) are maintained (Whipple 2017; Xiao et al. 2022). In *Brassicaceae*, the suppressed bract directly subtends the flower. Despite these differences, two common points are shared. First, bract reduction is not total. Morphological deformations (Kwiatkowska 2006) and localised gene expressions, such as *A. thaliana FILAMENTOUS FLOWER* (*FIL*) or its maize ortholog *Zea mays yabby15* (*Zyb15*), indicate that a bract domain forms but fails to outgrow (Long and Barton 2000; Dinneny et al. 2004; Whipple et al. 2010). In *A.*

thaliana, this domain is incorporated in floral tissues, remaining cryptic (Heisler et al. 2005; Goldshmidt et al. 2008). Second, in both families, mutants can restore a bract from the cryptic domain. This suggests that a gene regulatory network (GRN) actively suppresses bract outgrowth in this domain. In *Poaceae* model plants, bract regain in mutants is often interpreted as a heterochrony, or a change in developmental timing (Alberch et al. 1979). Bracts are compared to leaves produced during juvenile phases, so the persistence of this developmental program in the inflorescence suggests a 'prolonged vegetative phase' (Itoh et al. 1998; Kawakatsu et al. 2006; Chuck et al. 2007; Kawakatsu et al. 2009; Chuck et al. 2010; Wang et al. 2021). This hypothesis, however, does not offer clear insights into the precise mechanisms controlling bract regain in mutants, nor into the evolutionary scenario of bract loss in *Poaceae*.

Studies on bract mutants in *Poaceae* and *A. thaliana* have identified two GRNs controlling bract suppression. In *Poaceae*, the GRN is organised around *NECK LEAF1 / TASSEL SHEATH1 / THIRD OUTER GLUME1 (NL1/TSH1/TRD1*, or *NTT)* in rice, maize and barley respectively (Wang et al. 2009; Whipple et al. 2010; Houston et al. 2012). Loss-of-function mutants in grass species produce bracts (Whipple et al. 2010; Wang et al. 2021), but not in *A. thaliana* mutants of the orthologous gene *HANABA TARANU* (*HAN*) (Zhao et al. 2004). Upstream, NTT is directly regulated by *SQUAMOSA PROMOTER BINDING PROTEIN LIKE* (*SPL*) transcriptional regulators (Wang et al. 2009; Chuck et al. 2010; Chuck et al. 2014), themselves targeted by microRNA156/529 (miR156/529) (Chuck et al. 2007; Wang et al. 2021). The miR156/SPL balance regulates phase transitions from vegetative to reproductive stages in angiosperms (Wu and Poethig 2006; Wang and Wang 2015), providing a genetic module controlling heterochrony in plants (Buendía-Monreal and Gillmor 2018). This supports the interpretation that bract regain in mutants is a heterochronic phenotype. Downstream, NTT influences genes involved in hormone signalling, meristem and boundary identities, or leaf development (Xiao et al. 2022). Yet, few direct NTT-target genes have been identified, such as the *PLASTOCHRON1* (*PLA1*) and *PLA2* genes in rice (Wang et al. 2021). These genes encode two enzymes whose function has not been clearly identified (Miyoshi et al. 2004; Kawakatsu et al. 2006). Hence, NTT-downstream mechanisms of bract repression need clarification.

In *A. thaliana*, bract mutants revealed different genes from the *Poaceae* orthologs, all connected to the floral meristem identity (FMI) pathway. This genetic program specifies a floral rather than a shoot identity (Weigel 1995). Impairing FMI leads to flower-to-shoot conversions by restoring vegetative hallmarks into flowers: perturbed floral organ identity and phyllotaxis, internode elongation, indeterminacy and also, bract outgrowth. In *A. thaliana*, FMI relies on a complex gene regulatory network orchestrated by the transcription factor *LEAFY* (*LFY*) (Siriwardana and Lamb 2012): *lfy* mutants fail to produce proper flowers and show diverse bract outgrowths (Schultz and Haughn 1991; Weigel et al. 1992). Other FMI-related transcription factors also cause bract de-repression when mutated alone or in combination, suggesting they also act as bract-repressors: *UNUSUAL FLORAL ORGANS (UFO)* (Levin and Meyerowitz 1995; Hepworth et al. 2006), *APETALA1* (*AP1*)(Irish and Sussex 1990; Bowman et al. 1993), *BLADE ON PETIOLE1 (BOP1)* and *BOP2* (Hepworth et al. 2005; Norberg et al. 2005; Xu et al. 2010; Chahtane et al. 2018), *PUCHI* (Karim et al. 2009), *LATE MERISTEM IDENTITY 1 (LMI1)*, *AGAMOUS-LIKE 24 (AGL24)*, *SHORT VEGETATIVE PHASE (SVP)*(Xu et al. 2010; Grandi et al. 2012), *SUPPRESSOR OF CONSTANS 1 (SOC1)*, *SEPALLATA3 (SEP3)* (Liu et al. 2009), *FRUITFUL (FUL)* (Melzer et al. 2008; Balanzà et al. 2014), *TERMINAL FLOWER 1 (TFL1)* (Shannon and Meeks-Wagner 1991; Penin 2008) and *FILAMENTOUS FLOWER (FIL)* (Levin and Meyerowitz 1995; Sawa et al. 1999; Siegfried et al. 1999). Fewer genes have been identified as promoting bract outgrowth, such as *JAGGED* (Dinneny et al. 2004; Ohno et al. 2004), *AINTEGUMENTA* (*ANT*) and *AINTEGUMENTA-LIKE6* (*AIL6*) (Manuela and Xu 2024 Mar 28). In all these studies, bract de-repression is accompanied by pleiotropic phenotypes affecting flowers, branching or flowering time. Bracts, together with chimeric shoot-flowers, can also be induced in wild-type *A. thaliana* under specific light treatments (Hempel and Feldman 1995; Hempel et al. 1998). Finally, the genetic ablation of flowers induces bract outgrowths (Nilsson et al. 1998). Altogether, this suggests that FMI establishment is responsible for bract repression, although the precise mechanisms remain unclear.

To summarise, thanks to bract mutant studies, current models propose different GRNs to acquire the ability to suppress bract, either from boundaries in *Poaceae* or from flowers in *Brassicaceae*. In this latter case, it is unclear how FMI genes mostly expressed in flowers act

non-cell autonomously on the bract domain. Also, how this network acquired this new function remains to be determined.

This study revisits bract inhibition in *A. thaliana* with natural variation. Important differences suggest that the bracts naturally forming at the base of inflorescences involve developmental mechanisms distinct from mutant bracts and that may be more similar to bract-bearing species. Using two accessions, we mapped this heritable trait to four Quantitative Trait Loci (QTL). Transcriptomic profiling of bract-producing meristems indicates that during floral transition, the stage at which bract develops, the meristematic transcriptomes of the two accessions diverge the most, with numerous desynchronisation of gene expression relative to the flowering event. Challenging the model that FMI genes inhibit bracts, our results question whether changes in the timing of gene expression may play a role in canalising phenotypes during floral transition and in the evolution of bract loss.

Materials and Methods

Plant growth conditions

Seeds were sown on peaty-clay soil, stratified at 4°C for at least two days, and watered with fertiliser (18-10-18 N-P-K) under LED lighting (sunlight spectrum NS12, 150 µmol.m-2.s-1). Three different day/night regimes were used in the experiments: short-days (SD) with 8h light and 16h dark; long-days (LD) with 16h light and 8h dark and continuous light (CL) with 24h light. Temperature and humidity are controlled as follows: 22°C and 60% humidity during light for LD and CL conditions, and 18°C and 70% humidity constantly in SD and during night time in LD. For the Bulk Segregant Analysis and the RNAseq time course, plants were grown 20 days in SD before switching to LD. For the RIL phenotyping assays, plants have been directly cultured in LD.

Plant materials

A. thaliana natural accessions and associated RILs were obtained from the Versailles *Arabidopsis* Stock Centre (VASC), *Col-0*: 186AV, *Tsu-0*: 91AV, RIL set name: 3RV. F1 and F2 plants used for the BSA were generated by crossing the parents *Tsu-0* and *Col-0* in both directions. The following strains were obtained from the NASC and are in *Col-0* background if not otherwise mentioned: *ufo-1*: N16361 (*Col-2* background); jag-5d: N9506 (background: *Col-0 gl1 pop1*); *tfl1-13*: N6237; *tfl1-14*: N6238. *puchi-1*, *bop1-4* x *bop2-11* and *puchi-1 x bop1-4* x

bop2-11 (Karim et al. 2009), *lfy-12* (Maizel and Weigel 2004), *soc1-2* (Michaels et al. 2003) and *svp x agl24 x soc1* (Liu et al. 2009) were described previously. Plants expressing pLFY::2xmCherry-N7 ; 35S::Lti6b-YFP (in *Col-0* and *Tsu-0*) were generated for this study. *Tarenaya hassleriana* and *Gynandropsis gynandra* seeds were kindly provided by Pr Eric Schranz and Frank Becker, from Wageningen University (WUR, Holland). *Lunaria annua* and *Allaria petiolata* plants are spontaneous specimens found outside the laboratory, in France. The phylogeny of *Brassicaceae tribes* used in Fig. S1 is extracted from the Brassibase website (Kiefer et al. 2014).

Plasmid constructions and plant transformation

pLFY::2xmCherry-N7: since no polymorphism was sequenced in the *LFY* promoter between *Col-0* and *Tsu-0* accessions, a sequence starting at -2277pb upstream of the ATG was amplified by PCR from *Col-0* genomic DNA using 5'GGGGACAACTTTGTATAGAAAAGTTGATCCATTTTTCGCAAAGG and 5'GGGGACTGCTTTTTTGTACAAACTTGAATCTATTTTTCTCTCTCTCTCTATC primers. PCR fragments were purified and inserted into pDONR P4-P1R with a gateway BP reaction. This plasmid was then recombined in a three-fragment gateway reaction with 2xmCherry pDONR211 and N7-tag pDONR P2R-P3 (containing the nuclear tag N7 and a stop codon) and the destination vector pK7m34GW. 35S::Lti6b-YFP: a pDONR P2R-P3 plasmid containing the sequence of the plasma-membrane protein Lti6b (Cutler et al. 2000) was recombined in a three-fragment gateway reaction with a 35S pDONR P4-P1R and the YFP pDONR P2R-P3 into the destination vector pB7m34GW. Both constructs were then transformed into *Agrobacterium tumefaciens* C58pMP90 strain by electroporation and transformed into both *Col-0* and *Tsu-0* plants by floral dipping (Clough and Bent 1998). For each construct-by-genotype combination, several independent transgenic lines were selected in T2 for a single insertion event based on 3:1 resistant:sensitive mendelian segregation of the resistance provided by the transgene. The expression patterns of pLFY were reproducible between selected lines and matched published data for *Col-0*. We were unable to get a 35S::Lti6b-YFP line with a membrane signal as strong in *Tsu-0* as in *Col-0* (Fig. 2 and S2). However, despite the weak YFP signal, the morphology of the tissue could still be captured.

Microscopic meristem imaging and image analysis

Meristems were imaged using a Scanning Electron Microscope (Hirox 3000 SEM), or with a confocal microscope Zeiss 700 LSM, according to the manufacturer's instruction and without prior fixation. Multitrack sequential acquisitions were performed as follows: YFP, excitation wavelength (ex): 488 nm, emission wavelength (em): 300–590 nm; mCherry, ex: 555 nm, em: 300–620 nm. Detection wavelengths and laser power were identical for *Col-0* and *Tsu-0*, PMT voltage was identical for mCherry to allow comparisons of pLFY signal intensity in the two genotypes. The YFP PMT voltage was optimised on each plant. Confocal images were processed using imageJ (Schneider et al. 2012): maximum projections of mCherry channel and 16-bit-transformed standard deviation projections of the YFP channel were merged in a composite image. mCherry intensities were unchanged while brightness and contrast of the YFP channel were optimised on each plant to provide the best morphological outlines of the tissues.

Macroscopic plant phenotyping

Macroscopic pictures were taken using different devices, according to the manufacturer's instructions: Keyence VHX-900F, Canon EOS 450D camera, camera device of a Samsung Galaxy A10 and a Ulefone Armor X5 pro.

Phenotypic measurements

Basal bract score was determined by counting all bracts in the main stem and cauline branches, normalising by the total number of branches (excluding rosette branches, **Fig. 1E**); the inspection was limited to the first five flowers, especially for mutants. The number of bracts was counted after internodes elongation on the last upper cauline branch to ensure bracts were visible to the naked eye. Flowering time was measured with different methods (mentioned in the main text): the number of days from the start of transfer to in growth chambers to the day of bolting, the day when the first flower blooms (open petals), or as the cumulated number of leaves (rosette only or rosette and cauline). For plastochron measurements, several plants of both genotypes were synchronised and grown in the same condition. Each sampling day after transfer to a long day, 5 to 10 plants were randomly dissected under a binocular dissecting scope, removing and counting all organs (leaves or flowers) from the first leaf to the youngest organ visible on the main meristem. The youngest

198 organs were counted as soon as they were separated by a boundary (corresponding to stage-2
199 flowers as defined by (Smyth et al. 1990).

200 **DNA extraction and sequencing for Bulk Segregant Analysis (BSA)**

201 For the BSA, an F2 mapping population of 684 plants was generated by crossing (*Col-0* x *Tsu-0*)
202 in both directions. The bulk segregant analysis was split into four replicates. A 1cm² leaf sample
203 was sampled for each F2 plant, kept at -20°C and genomic DNA was extracted individually if the
204 plant was selected in one of the bulk. Genomic DNA of 56 and 17 plants were selected and
205 pooled in the bulks of low and high bract-score plants, respectively. The genome of the parental
206 lines was re-sequenced using genomic DNA from bulk *Tsu-0* and *Col-0* seedlings, respectively.
207 All genomic DNAs were extracted and purified using a CTAB-based protocol (cetyl
208 trimethylammonium bromide), following instructions as in (Healey et al. 2014).
209 Each DNA bulk was prepared by pooling the genomic DNA of selected plants in equal quantities,
210 to reach a final concentration between 13 and 25 ng/µl. Pooled DNA bulks and parental DNA
211 were used to prepare libraries and sequenced on BGISEQ-500WGS according to the
212 manufacturer's instructions, yielding 5 Gb data of 100bp paired-end reads per library (target
213 coverage of 40X).

214 **DNA sequencing analysis and genomic variant analysis**

215 Sequencing data consists of two parental plus two bulks of sequencing data. A genomic variant
216 analysis was performed on each dataset following the workflow of short variant discovery
217 previously described in (Besnard et al. 2020). This resulted in four gVCF files (one per sample)
218 generated by the HaplotypeCaller tool of GATK (v3.8, McKenna et al., 2010). TAIR10 was used
219 as the *A. thaliana* reference genome. Then, the two parental gVCF were first joint-genotyped
220 using GATK's tool GenotypeGVCFs to emit a common vcf file for the two samples. This file was
221 used to select a list of specific SNPs and small indels of *Tsu-0* (91AV stock) versus *Col-0* (186AV
222 stock), filtering for positions with coverage metric DP>10. This reference list of *Tsu-0*
223 polymorphisms was then used as the --dbsnp option in a second pass of joint genotyping using
224 all four gVCF as input (two parental samples plus the two bulks) to emit a common vcf file.
225 Finally, relevant polymorphic positions from the reference list in the two bulks were selected
226 after filtering for a depth ≥3.

QTL mapping from Bulk Segregant Analysis

QTL identification was carried out using the QTLseqr package (Mansfeld and Grumet 2018) according to user instructions. After filtering data with the following parameters (refAlleleFreq = 0, minTotalDepth= 10, maxTotalDepth = 90, minSampleDepth = 10, minGQ= 99, depthDifference = 15), the deltaSNP index (Takagi et al. 2013) was generated and loci that reached the ~95\% confidence interval were retained.

QTL mapping using Recombinant Inbred Lines

Genotyped RILs from *Col-0 x Tsu-0* (3RV) are publicly available in the VASC. Based on BSA results, a panel of 55 RIL were selected from their known genotypes on chromosomes 1 and 5 using GGT 2.0 software (van Berloo 2008). The detailed genotypes of each line used in this study are available in **Table S6**. The presence of basal bracts was quantified in each line using the bract score. QTL mapping was performed with R/qtl software according to user instructions (Broman et al. 2019): we used the scanone function with the mean value of the bract score for the 55 tested RILs as a trait and significant thresholds were computed by setting a permutation number to 2000. For the bract score, the “non-parametric” (np) statistical model was used while for paraclade number, we used a normal model implemented with the hk method. To look for QTL interactions, the scantwo function was used with the normal model and the hk method since the np model is not implemented for this function. MQM was performed with default parameters. The (broad-sense) heritability for the bract score was defined as $H^2 = (var_T - var_E) / var_T$, with var_T and var_E being the total and environmental variance, respectively. var_T was computed as the total variance of the bract score of each plant over the entire QTL mapping dataset (1830 RIL plants and 780 control parents split over 12 experiments) while var_E was computed as the pooled variance of the line variances (computed over all plants of a line across experiments). Confidence intervals of H^2 were provided by bootstrapping 70% of the strain 1000 times.

KASP genotyping

We selected 19 new genotyping markers from the 140SNPvCol marker set (Lutz U. et al. 2017) to cover the two large QTLs mapped in chr1, 1a and 1b (**Fig. S5B**) and corresponding kompetitive allele-specific PCR (KASP) oligos were ordered to Biosearch Technologies™ LGC Ltd.

To further reduce the intervals, we designed two new SNP markers targeting *Tsu-0* polymorphisms identified in our whole-genome re-sequencing data. Specific KASP oligos (three per SNP) were designed by LGC from the 100-bp sequence surrounding the SNP. All 21 new markers (**Table S7**) were validated on parental genomic DNA (*Col-0* and *Tsu-0*) in a KASP assay before their use with recombinant inbred lines. Clean genomic DNA from CTAB-based extraction was used for all samples. For each marker, 2.5 µL of DNA (diluted to a final concentration of 5 ng/µL), 2.5 µL of KASP-TF V4.0 2X Master Mix low ROX and 0.07 µL KASP assay mix were mixed in 384-well plates and the genotyping assays were run in a QuantStudio 6 Flex (Applied Biosystems), using standard user guidelines for thermal cycling and final fluorescence analysis.

Fine mapping using Heterologous inbred families

Using F6 genotyping data for the 3RV RIL set from the VASC, we selected 3 RILs heterozygous in a region overlapping QTL1a, QTL1b and the interval in-between: RIL 334, 488 and 478, respectively (**Fig. 3** and **Fig. S5**). For RIL 334 and 488, we genotyped by KASP 160 segregating F8 progenies and selected 5 and 8 plants, respectively, with homozygous recombination inside the QTL region under study. For RIL 478, we genotyped 20 plants and selected only one; genotyping reactions were performed using PCR primers designed to amplify the published marker of the VASC (Simon et al. 2008)(**Table S8**) and the results were read by Sanger sequencing. All selected F8 plants were selfed to generate an inbred line of a fixed genotyped (F9), the collection of F9 inbred lines forming a Heterologous Inbred Family (HIF). HIF lines (with at least 20 plants per line) were phenotyped for the bract score with parental control in the same experiment.

Biological sample preparation for the transcriptome time-series profiling

After 20 days in SD, *Tsu-0* and *Col-0* meristems were dissected every day in LD conditions, in order to capture the precise developmental stages (especially stages T and F, see below). The mutants *lfy-12*; *puchi1 x bop1 x bop2*; and *jag5-D* meristems were dissected every day starting from 1 week after LD transfer to target the stage F. Three independent biological experiments were performed with 5 to 11 meristems per replicate. Stages are defined as follows: V, the day when plants were transferred to LD from SD; L, after 4 to 5 days of LD (identical for both *Col-0* and *Tsu-0*, which have the same meristem shape at this time); T, the main meristem enlarges

and domes, (Kwiatkowska 2008; Kinoshita et al. 2020), and lateral meristems starts being visible at the axils of young leaf primordia; F, all young organs in the meristems were identified as flowers (note that this stage occurred several days before bolting). Stage F in mutants was defined when several rounded primordia become visible at the SAM (that will become branch-like flowers or only branches). Dissections were performed from 9:00 a.m. to noon, by alternating between *Tsu-0* and *Col-0*. Micro-dissected meristems were snap frozen in liquid nitrogen and stored at -80°C until RNA extraction. To avoid the induction of stress-related gene expression, meristem dissection did not exceed 3 min between the first organ removal and freezing. For each replicate, pooled meristems were ground with a RockyII tissue lyser according to the manufacturer's instructions. RNA was extracted using the PicoPure RNA Isolation Kit (Arcturus, Catalog KIT0202) according to the standard protocol. RNA concentration ranged from 3 to 64 ng/µl (average 23ng/µl), with a RIN value between 5.6 and 7.6 (average 6.8).

RNA-sequencing

Library preparation was made using NEBNext® Ultra™ II Directional RNA Library Prep Kit for Illumina (New England Biolabs); NEBNext® Poly(A) mRNA Magnetic Isolation Module (New England Biolabs); and NEBNext® Multiplex Oligos for Illumina (Index Primers Sets 1, 2 et 3), from 40ng of RNA and sequenced using the NextSeq500 (Illumina). Sequence quality was controlled using the Sequencing Analysis Viewer, sequences that did not pass the quality filter were removed. Following QC an average of 43 million sequences per sample was achieved.

RNA-seq analysis (pre-processing procedures)

Quality filtering using Trimmomatic (Bolger et al. 2014) retained for all samples 96% of the reads, which were aligned to TAIR10 genome using STAR (Dobin et al. 2013) with the following parameters: non canonical splice junctions were removed, multi-mapping reads were limited to 10, and only reads mapped once were considered to determine splicing junctions. Between 88 and 97% of the reads were mapped to a simple locus. Normalisation of read counting was performed using the R Bioconductor packages DESeq (Love et al. 2014), with the following parameters: genes for which the total number of reads was below 10 were discarded, and data were transformed with Variant Stabilising Transformation (VST) function (Anders and Huber

2010), to harmonise the variance. Consistency between biological replicates was verified using a Principal Component Analysis on all samples with VST-transformed data.

RNA-seq analysis: Differential Gene Expression (DGE) analysis

Differential analysis was performed using the R Bioconductor package edgeR (McCarthy et al. 2012). Reads were first normalised using TMM (Trimmed mean of M-values) to reduce library-specific biases. Normalisation factors were between 0.94 and 1.049. A generalised linear model was applied for the analysis of differentially expressed genes (DEG). Three types of DEG analysis were considered: DEG at each stage between the different genotypes, DEG between the stage within the same genotype, and DEG across all conditions (stages and genotypes). Multiple DEG analyses were corrected using Benjamin-Hochberg correction, and genes with a p-value < 0.05 were retained.

RNA-seq analysis: clustering gene expressions correlating with bract presence

To identify candidate genes that may act as positive or negative bract regulators (see **Figure 5G**), we first calculated the minimum and maximum expression levels among stages with and without bracts. If the minimum expression level in the stages with bracts was greater than or equal to the maximum expression level in the stages without bracts, the genes were considered positive bract regulators. If the maximum expression level in the stages with bracts was lower than or equal to the minimum expression level in the stages without bracts, the genes were considered positive bract regulators. If neither of these conditions were satisfied, genes were discarded.

Temporal registration of gene expression dynamics

To align gene expression profiles of *A. thaliana Tsu-0* (query data) with *Col-0* (reference data), we utilised the curve registration method in the R package greatR (Kristianingsih 2024). This approach involved shifting the gene expression profiles of *Tsu-0* across developmental stages (V, L, T, F) using shift factors ranging from -1 to 1; a stretch factor was not applied due to the two datasets being over similar times. The optimal shift parameter for each gene pair was identified by maximising the log-likelihood. The fit with the best registration factors for each gene was then compared to the fit with a non-registered model (without transformation) using the Bayesian Information Criterion (BIC) statistic. A lower BIC score for the registered model

(with transformation) indicated that the gene expression dynamics of *Tsu-0* and *Col-0* were similar, and the expression profile differences could be resolved through registration. Conversely, a higher BIC score suggested that the profiles were best described by two individual curves, i.e. not aligned. Prior to transformation, gene expression levels in both datasets were centred and scaled using the z-score scaling method. The standard deviation value for the replicates at each time point was set to 0.01.

GO terms analysis

GO term enrichment analyses were performed using either the 'Single Enrichment Analysis' tool from AgriGOv2 (Tian et al. 2017) with default parameters (Fisher's test with Yekutieli adjustment method) or clusterProfiler 4.0 (Wu et al. 2021) with default parameters (enrichGO and simplify functions with "BH" adjustment method). The Rich factor was computed by dividing the number of genes associated with a GOterm ("Count") by the numerator of the "BgRatio" computed by the enrichoGO function.

Gene selection inside genetic mapping intervals

The R library 'GenomicFeatures' (Lawrence et al. 2013) was used to import gene information from the most recent annotation file of *A. thaliana* at the gff format (Cheng et al. 2017). Custom R scripts were used to intersect all gene loci falling within genetic mapping data and provide for each gene information from RNA-seq analysis and genomic variant analysis (see Table S1 and Table S2). We used snpEff v5.0d (Cingolani et al. 2012) and its putative functional categories (HIGH/MODERATE/LOW/MODIFIER) to predict the functional impacts of the genomic variants over regions covering each annotated gene of the interval, including promoter (2 kbp upstream of the transcriptional start site) as well as 500-bp downstream region in the case of miRNA. In Table S1 and S2, additional gene information was retrieved from ThaleMine (Pasha et al. 2020) and GO terms from the TAIR bulk data retrieval tool.

Data handling, data visualization and descriptive statistics

The R software was used (R Core Team 2018), especially the following packages: Bioconductor packages (Huber et al. 2015) for the analysis of omics data, especially GenomicFeatures, IRange (Lawrence et al. 2013), rtracklayer (Lawrence et al. 2009), clusterProfiler (Wu et al. 2021), limma (Ritchie et al. 2015), DESseq2 (Love et al. 2014), edgeR (Chen et al. 2016) and

org.At.tair.db (Carlson 2024); dplyr (Wickham et al. 2023), tidyr (Wickham et al. 2024) and reshape2 (Wickham 2007) for data manipulation and ggplot2 for almost all plots (Wickham 2016), with viridis and plasma (Garnier et al. 2024) for some colour optimization.

Text and english

Language correction software with artificial intelligence was occasionally used throughout the text to ensure correct spelling and grammar as well as the most comprehensible style possible.

Results

Transient bract formation during the floral transition is common among A. thaliana accessions

The typical *Brassicaceae* flower has no bract. Yet, a number of *Brassicaceae* species produce some bracteate flowers (i.e. with bracts) at the base of their flowering branch (a raceme) (**Fig. 1A** and **Fig. S1 A-D**), a common botanical trait in this family (Endress 2006; German et al. 2023). Hence, bract loss in *Brassicaceae* is incomplete, showing a reduction trend compared to its sister clade *Cleomaceae* (**Fig. 1A**, **Fig. S1E**). Mapping the presence of bracts among the *Brassicaceae* phylogeny does not reveal an evolutionary scenario (**Fig. S1A**). Some species display bracts up to the first half of the raceme (e.g. **Fig. 1A**), while others only have one or two bracts at the base (**Fig. S1 C, D)**, e.g. in (Al-Shehbaz 2015). While the reference *Col-0* accession of *A. thaliana* bears no bracts, we discovered that the natural *Tsu-0* accession displays bracts on the first one to five flowers of the raceme (**Fig. 1A**). Under a stereomicroscope, a gradient of bract outgrowth is visible, from fully developed bracts resembling the cauline leaves associated to branches, up to filamentous, short rudimentary structures (**Fig. 1B**). Using scanning electron microscopy, a mild swelling of the peduncle basis could sometimes be observed in *Tsu-0*, unlike *Col-0* smooth peduncle (**Fig. 1C**). In *Tsu-0*, bract development can thus be released to varying degrees in the first flowers of a branch, which we have termed “basal bracts”. Other genetically diverse natural accessions produce basal bracts, albeit at a highly variable rate (**Fig. 1D**) and without any clear correlation to geographic or genetic origins (**Fig. 1D, Fig. S1 F, G**). Interestingly, *Col-0* also produces basal bracts at a low frequency, typically on lateral branches. In general, we observed that basal bracts can develop at every flowering branch but with a

401 variable frequency, even within an accession and in fixed environmental conditions. To quantify

402 basal bracts, we

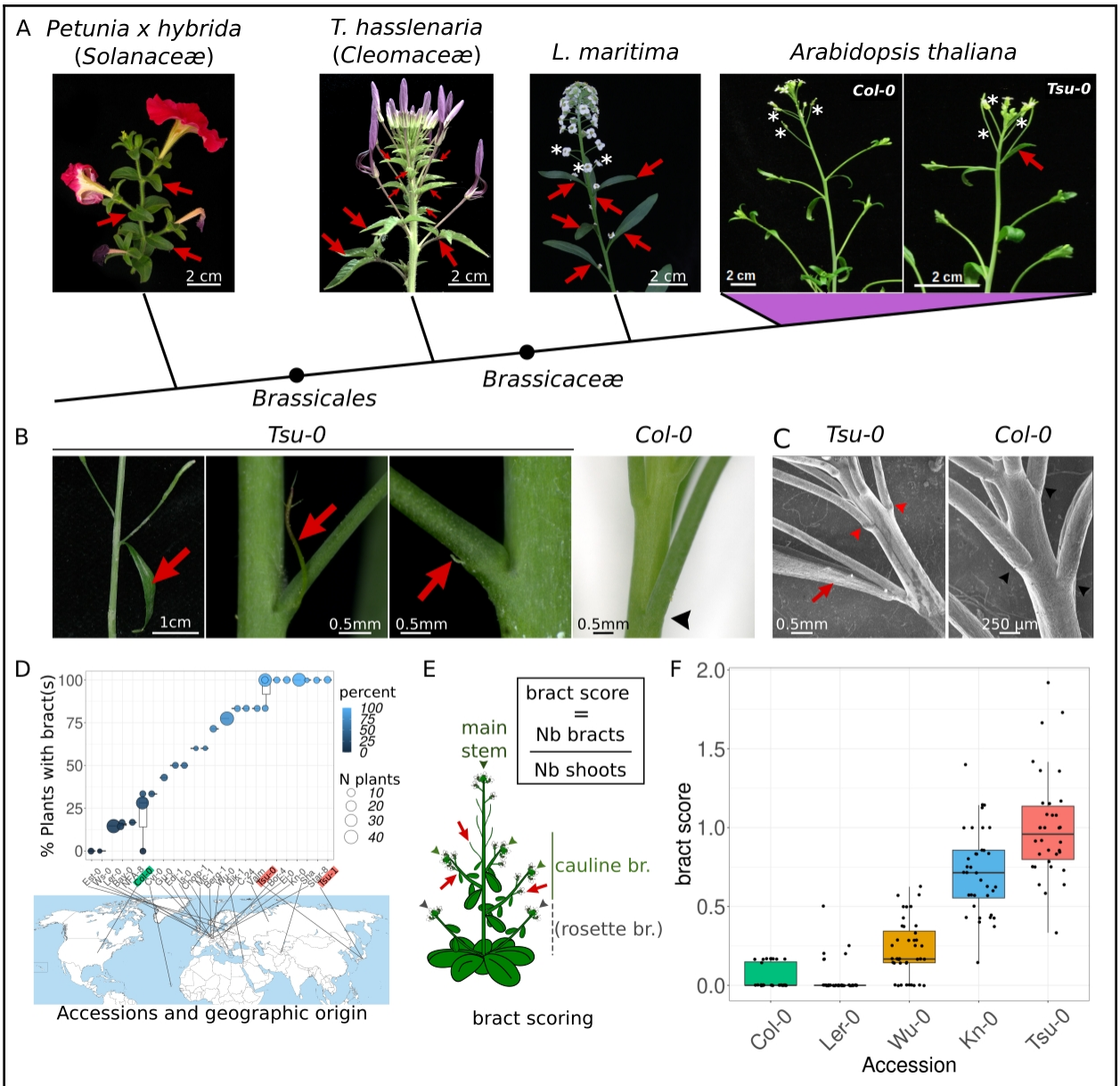

Figure 1: **The presence of basal bracts is a common, natural trait in *Arabidopsis thaliana* with quantitative variations among genetic backgrounds**. **A**, Examples of bracts (red arrows) in different angiosperms. *Brassicaceae* are mostly bractless but some species retain bracts at the base of inflorescence branches (e.g. in *L. maritima*). In *A. thaliana*, some natural accessions display basal bracts (e.g. *Tsu-0*) while others do not (e.g. *Col-0*). Schematic phylogenetic relationships are indicated with a cladogram below the pictures. White stars: first ebracteate flowers following previous bracteate flowers **B**, (from left to right) *A. thaliana*'s basal bracts can be true leaves or just small rudimentary filamentous structures at the base of the floral pedicel (red arrows). These structures are absent in younger flowers, as in the reference *Col-0* accession (rightmost panel, black arrowhead). **C**, Details of basal

bracts by scanning electron microscopy in a *Tsu-0* inflorescence tip (left panel), showing a bract on the first flower (red arrow) and swollen base of pedicels on the two following flowers (red arrowhead). Right panel: pedicels of *Col-0* plants do not show such structures (black arrowhead). **D**, Occurrence of basal bracts in different accessions, assessed by the percentage of plants with at least one basal bract in the inflorescence. Each dot is the average value of several plants (number indicated by dot size) of a scoring assay. A box plot indicates several assays per line and thicker horizontal black lines are the median value of all scoring assays (range 1-3) in the accession. *Col-0* and *Tsu* are highlighted in green and red, respectively. The geographical origin of each strain is located in the world map below. **E**, Definition of a quantitative bract score for a single plant (see main text for detail). **G**, Quantification of basal bracts in different accessions using the bract score.

defined a bract score (**Fig. 1E**) which captures both intra- and inter-genotype variations (**Fig. 1F**). *Tsu-0* and *Col-0* ranked respectively as high and low bract producers and were kept for further investigation.

Basal bracts develop with wild-type flowers and differ from known mutant bracts

To investigate basal bract development, we imaged the emergence of the first flower. Scanning electron microscopy revealed a sharp floral transition in *Col-0*: the last lateral meristem subtended by a cauline leaf is immediately followed by ebracteate (i.e. bract-less) flowers (**Fig. S2A-B)**. In *Tsu-0*, the first flowers produced after the last branch bear bracts or rudimentary bracts (**Fig. S2C-D)**. Their association with young flowers indicates that these bracts are not secondary outgrowth from mature floral peduncles. In bract-making species like the sister clade *Cleomaceae*, we observed that bract emerges before the flower (**Fig. S2E**). In *A. thaliana*, the abaxial position of bracts and their precocious development suggest that they are true de-repressed bracts. Given LFY's central role in suppressing bract development in *A. thaliana*, we question whether bracts form due to LFY perturbation at floral transition. Using a p*LFY* reporter line, we observed in both genotypes the same sharp activation of *LFY* transcription from the first flower onwards (**Fig. 2A-B**), regardless of bract presence in *Tsu-0* (**Fig. 2B-C**). Accordingly, *Tsu-0* bracteate flowers were wild-type, with a normal number of floral organs (**Fig. 2D**). This contrasts with reported bract mutants which presented severe phenotypes, such as loss of floral organs or lack of determinacy with branched flowers (**Fig. S3**). Interestingly, *pLFY* was also activated in the bract margins, albeit at lower

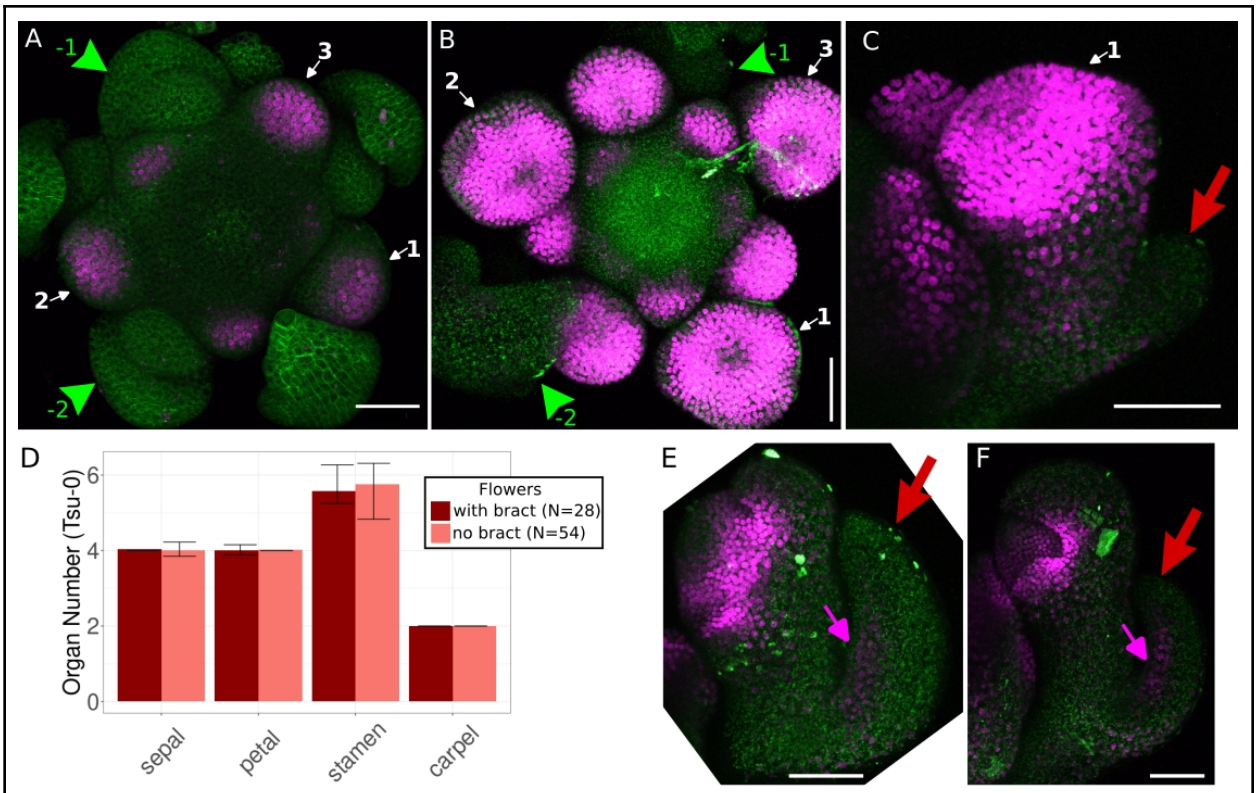

Figure 2: **Flowers bearing bracts express high levels of LFY and do not display mutant phenotypes**

A, B. Confocal live imaging of the main meristems of *Col-0* (**A**) and *Tsu-0* (**B**) plants at floral transition, expressing a pLFY transcriptional reporter (magenta) and a membrane marker (green) for morphology (top-view projections of stack acquisitions). Green arrowheads: branches, ordered with decreasing numbers from the floral transition; white arrows: flowers ordered with increasing numbers from the floral transition. In both genotypes, pLFY expression is absent from branch meristems and suddenly appears in the first flower onwards. Representative pictures of at least 6 plants per genotype captured at floral transition.

C, side-view of the first flower from image B (*Tsu-0*): a bract (red arrow) is visible on the abaxial side of this young flower.

D, Number of floral organs in flowers with (dark red) or without (light red) bract in *Tsu-0* plants.

E, F. Side views by confocal live imaging of *Tsu-0* flowers with bracts (red arrow) expressing the pLFY reporter (magenta) and the green morphological marker. Flowers show two developmental stages older than C and with increasing age from E to F, as shown by the growing abaxial sepal on top of the flower. pLFY is expressed at low levels in the bract margins (magenta arrow).

Scale bars: 50 µm

levels than in the floral meristems (**Fig. 2E-F**), contrary to the proposed role of LFY as a bract inhibitor. To better understand LFY contribution to basal bracts, we then re-examined bracts in mutants with lowered *LFY* expression: *lfy*, *ufo* (Hepworth et al. 2006) and *puchi x bop1 x bop2*

(Karim et al. 2009). As previously reported (Chahtane et al. 2018), bracts in these mutants were at the tip of old branches and more frequently on secondary than on main shoots (**Fig. S4 A-G**). In *Tsu-0*, however, basal bracts were limited to the first flowers at floral transition (**Fig. S4H**), with the same frequency on each shoot (**Fig. S4I**). In addition, at floral transition, these mutants produced branches typically lacking cauline leaves, called I* branches in the literature (Ratcliffe et al. 1998), which have been interpreted as flower-to-shoot transformations. The first determinate flowers coming after I* branches were also ebracteate (**Fig. S4 B, C**). Hence, at floral transition, loss of FMI gene function is sufficient to lose floral fate but not to restore leaf development, unlike at branch tips, suggesting *LFY* effect on bract formation is context-dependent. We further tested the effect of intermediate LFY expression levels by scoring basal bracts in *LFY//lfy-null* heterozygous plants (**Fig. S4J**). The meristem was sensitive to halving the genetic dose of *LFY*, as shown by the slight increase in the number of branches. However, all basal flowers were wild type and ebracteate, confirming that this range of variation in LFY levels does not affect basal bract formation. Other bract mutants rarely produce bracts at the base of inflorescence but either on each node (e.g. in *JAGGED* gain-of-function mutant) or at the tip of branches (**Fig. S5**). Although *tfl1* mutants produce frequent basal bracts, these are likely cauline leaves that initially subtended branches, which were later transformed into flowers, as suggested by the presence of a few lateral branches (**Fig. S5**). These phenotypic differences suggest the genetics of bract development in mutants differ from those in *Tsu-0*, which may be influenced by the particular context of floral transition. This first report of bracts associated with wild-type flowers in *A. thaliana* illustrates that flower and bract formation are not necessarily incompatible in this species, questioning the underlying developmental mechanisms.

Basal bract frequency is unaffected by variation in photo-induction or plastochron length, but shows complex correlations with flowering time

To characterise factors governing basal bract formation, we evaluated the effects of photo-inductions as reported by (Hempel and Feldman 1995; Hempel et al. 1998). In these seminal experiments, basal bracts were induced together with graded phenotypes of chimeric

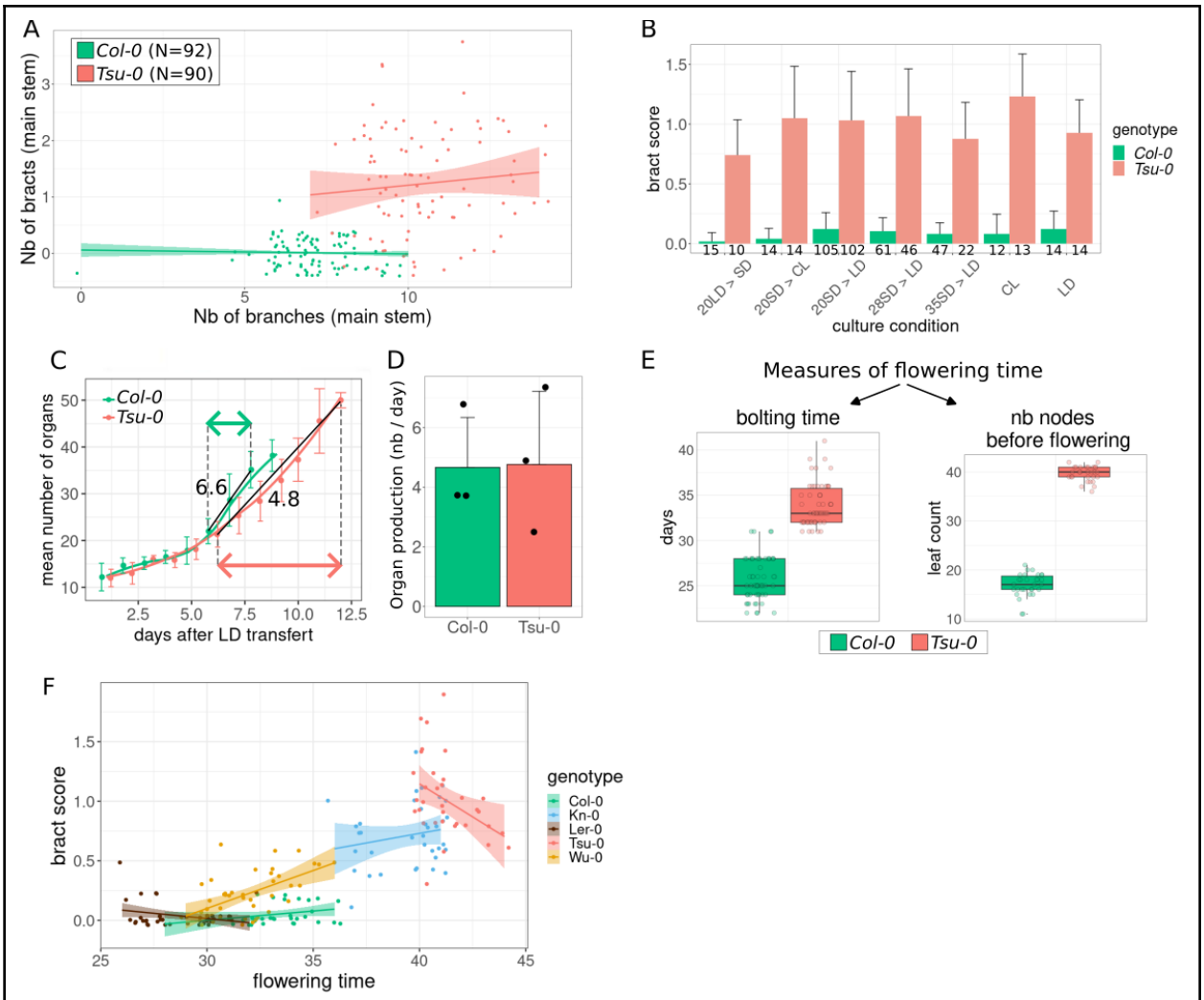

Figure 3: **Variation in natural basal bract frequency is not correlated with branch position, plastochron length or light conditions, but with variation in flowering time**

A, Correlation study between the number of lateral (cauline) branches and the number of bracts on the main stem only in *Col-0* and *Tsu-0* plants (green and red, respectively). (Pearson test, p-value > 0.1).

B, Effect of different light regimes on bract scores in *Col-0* and *Tsu-0* plants (green and red, respectively). LD and SD stand for long- and short-day conditions, respectively and CL stands for continuous light (see methods). Numbers (e.g. 20SD > LD) indicate the number of days in the first condition before transfer to the second. The number of plants scored is indicated below each bar.

C, Cumulated production of organs over time for *Col-0* and *Tsu-0* plants counted in microdissected shoot apices (green and red, respectively, each time point averaging 5 to 10 plants): the time window when plants make the floral transition is indicated by a horizontal arrow and vertical dashed lines. The rate of organ production (inverse to the plastochron) in this period is computed from the local slope of the curve. Plants were cultured for 21 days in short-day conditions before transfer in long-day (LD) conditions (see methods).

D, Result of three independent experiments of plastochron measurements at flowering

transition (see also fig. S5).
E, Differences in flowering time between *Col-0* and *Tsu-0* accession measured as bolting time in days (left) or as the number of vegetative nodes (rosette leaves and cauline leaves/branches) before the first flower on the main stem. Plants grown in LD conditions, N = 58 plants per genotype in two independent replicates.
F, Correlation study between the bract score and the flowering time (assayed when the first flower opens) in different accessions, labelled with different colours. Each dot is a plant and a linear regression standard deviation is computed for each accession.

shoot-flowers in natural accessions. These results lead to the "conversion" model, where a strong photo-induction converts a young branch meristem (already subtended by a leaf) into a bracteate flower. However, in *Tsu-0*, we never observed such shoot-flowers chimaeras (**Fig. 1, 2 and S2**) nor a negative correlation between the numbers of bracts and cauline branches (**Fig. 3A**), supporting that *Tsu-0* bracts are not linked to shoot-to-flower conversions. While Hempel and Feldman observed flower formation in hours after their strong photo-induction, our floral transition occurred at least one week after transfer to long days (**Fig. 3C**), suggesting milder photo-inductive signals in our growth conditions. However, further varying photo-inductive conditions did not affect the bract score in *Tsu-0* nor in *Col-0* (**Fig. 3B**). In the conversion hypothesis, bract formation is promoted by shorter plastochrones, the time between two lateral meristem initiations. Indeed, young meristems can be converted into flowers during a short time window: with short plastochrones, young branch meristems sensitive to floral conversion are frequently produced. In addition, the *plastochron1/2/3* mutants in rice have a shorter plastochron (Miyoshi et al. 2004; Kawakatsu et al. 2006; Kawakatsu et al. 2009) and make bracts. We evaluated precisely the plastochrones of *Col-0* and *Tsu-0* plants during the floral transition by micro-dissecting shoot apices in time series. Despite the variability, we found no consistent shorter plastochron in *Tsu-0* compared to *Col-0* (**Fig. 3C, D; Fig. S6A**). A clear difference between *Tsu-0* and *Col-0* is their flowering time, which happens in older *Tsu-0* plants in absolute time or in developmental time, and consistently across conditions (**Fig. 3E** and **Fig. S6B**). A panel of five accessions showed a global positive correlation between flowering time and bract score when comparing genotypes (**Fig. 3F**). However, within an accession, the correlation can be negative (e.g. in *Ler* and *Tsu-0*), suggesting more complex relationships with

flowering time. Altogether, our results indicate that basal bract formation in *Tsu-0* is not linked to variation in light or productivity (plastochrone) but may be influenced by flowering time.

Basal bract development is controlled by multiple QTLs suggesting new genetic mechanisms

To identify the genetic determinism of basal bracts, we conducted quantitative genetics using crosses between *Tsu-0* and *Col-0*. F1 progeny showed intermediate bract scores while F2 bract scores spread within the parental range, with a distribution that does not indicate a simple monogenic trait (**Fig. 4A and Fig. S7A**). Bulk Segregant Analysis (BSA) with mapping-by-sequencing identified four quantitative trait loci (QTL): two on chromosome 1 and two on chromosome 5 (**Fig. S7B, C**). The large spread of F1 phenotypic values constrained F2 plant selection with few plants in the high-score bulk and possibly spurious homozygous in the low-score bulk. These two limits may explain the large intervals obtained. To overcome the uncertainty on the phenotypic value attributed to an F2 genotype, we then used Recombinant Inbred Lines (RIL), which allowed averaging of bract scores across isogenic plants. Using an existing RIL set (Simon et al. 2008), we measured the average bract scores of several lines (**Fig. S8A**) for which we checked the absence of recombination bias (**Fig. S8B**). The heritability of bract score was high among RIL (65.45% +/- 1.7) and single QTL scanning mapped four peaks: two most significant on chromosome 1 (named 1a and 1b) and two less significant on chromosome 5 (named 5a and 5b; **Fig. 4B**). Consistent with the BSA result, this analysis provided slightly different QTL positions and shorter intervals. A two-QTL scan suggested additive effects between QTLs 1a and 1b (**Fig. S8C**). To confirm and reduce the intervals of these two major QTLs, we used two RILs identified as heterozygous in a region overlapping with these QTLs at F6 generation (**Fig. 4C-H**). F8 plants from these RIL were re-genotyped at a higher density with new genetic markers (**Fig. S9A, B**) to select recombining intervals homozygous for either allele of the two parents (**Fig. 4D, G**). Selected plants founded new lines forming a heterologous inbred family (HIF) with identical genotypes except in a small interval, which allows testing the effect of alleles in that region only. Scoring bract scores among HIF confirmed

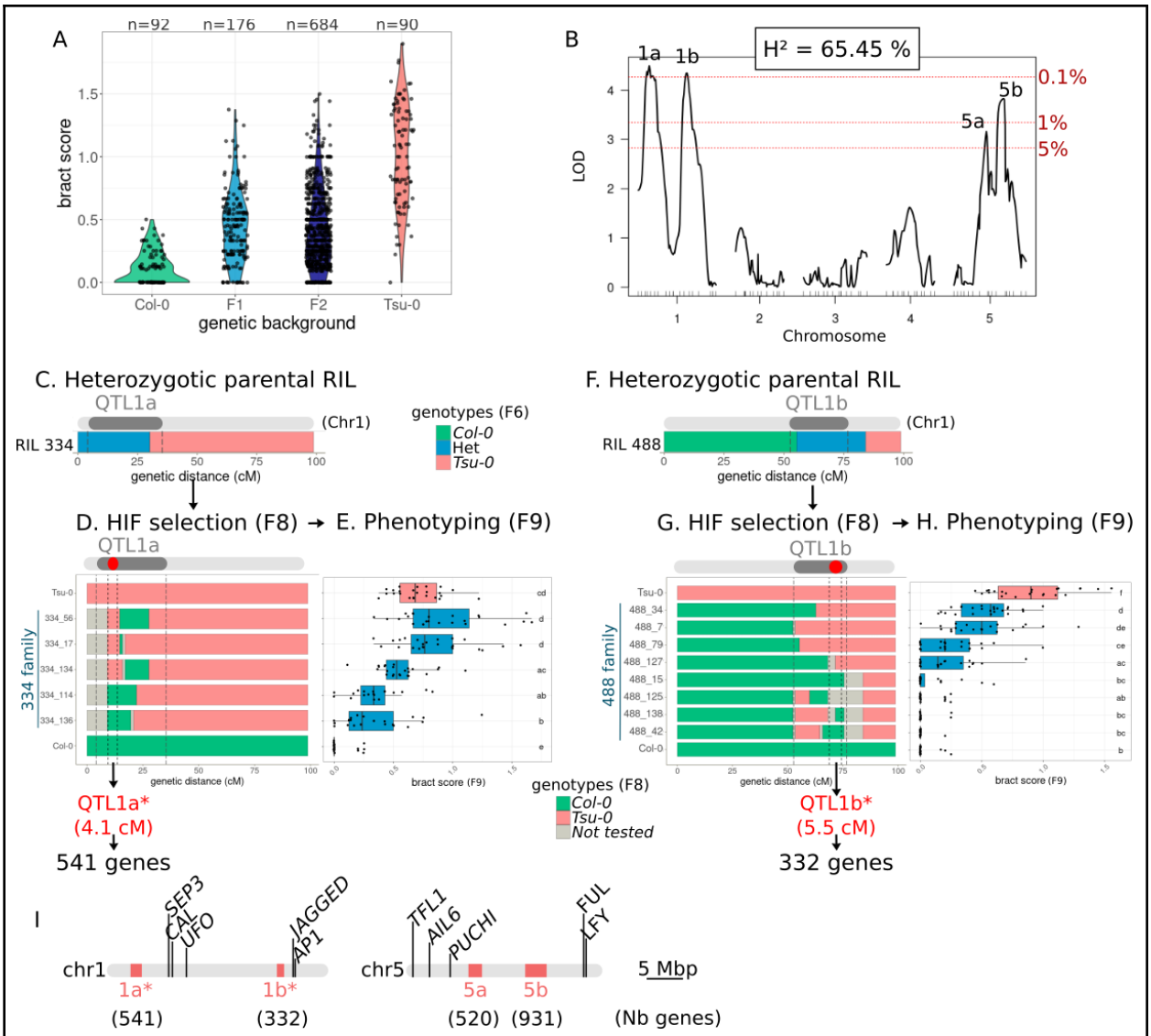

Figure 4: **Identification of 4 major QTLs controlling basal bract formation in *Tsu-0* suggests unknown genetic pathways**. **A**, Genetic transmission of bract score in F1 and F2 hybrids from a cross between *Col-0* and *Tsu-0* parent plants. **B**, QTL mapping for bract score in a set of RILs identifies four putative QTLs, two in chromosome 1 (1a and 1b) and two in chromosome 5 (5a and 5b). Dotted horizontal red lines indicate three different significance thresholds computed from 2000 permutations. On top of the graph, H^2 indicates the (broad-sense) heritability of the bract score computed among the RIL set. **C**, Genotype of the F6 generation of the line RIL334 in chromosome 1, showing a heterozygotic region overlapping with QTL1a. **D**, Chromosome 1 genotypes of selected lines forming a heterologous inbred family (HIF) obtained from RIL334 after two more generations of selfing (F8). **E**, Box plots of bract scores of the different lines from the "334 family" (blue boxes) with parental controls (*Col-0*: green, *Tsu-0*: red, N > 20 plants per line). Segregating bract scores within the family map a narrower region, QTL1a*, spanning 541 annotated genes. **F**, Genotype of the F6 generation of the line RIL488 in chromosome 1, showing a heterozygotic region overlapping with QTL1b. **G**, Chromosome 1 genotypes of selected HIF lines obtained from RIL488 at F8

and (**H**) a box plot of their bract scores (blue boxes), with parental controls (*Col-0*: green, *Tsu-0*: red, N > 21 plants per line). This maps a narrower region, QTL1b*, spanning 332 annotated genes. In E and H, lines not sharing the same letter(s) are statistically different (posthoc Tukey analysis with 0.05 sign. level from a glm of bract scores fitted with a quasi-poisson distribution). **I**, Final genetic mapping of the 'basal bract' trait in *Tsu-0* and the location of genes reported to impact bract development in previous mutant studies.

both QTLs and mapped them to smaller intervals named 1a* and 1b*. Additive effects of QTL 1a and 1b appeared when *Tsu-0* allele in 1b* was combined with *Col-0* allele in 1a*, the bract score reaching about half of the *Tsu-0* parent bract score (see in 488 families, **Fig. 4G, H**). However, *Tsu-0* parent score is tied only when both QTLs bear *Tsu-0* alleles (see in 334 families, **Fig. 4D, E**). As a control, we generated a HIF to test the region between 1a and 1b and demonstrated that it did not influence the bract score (**Fig. S9C-E**). However, mapped intervals remained large (4.1 to 11.8 cM), containing many genes (332 to 931, 2324 annotated genes for the four QTL, **Fig. 3I** and **Table S1**). The parental accessions that we re-sequenced differ by over 770,000 small genomic variations (SNPs and indels), with more than one variation every 175 bp on average, leaving few invariant genes to exclude (**Table S1**). Interestingly, known bract-related genes were absent from the QTLs (**Fig. 4I**).. However, a careful RIL phenotype inspection provided additional hints into the developmental pathways possibly involved in *Tsu-0* basal bract formation. First, we observed that the cauline branch number positively correlates with the bract score and QTL1b overlaps with a QTL controlling cauline branch number (**Fig. S10**). This suggests that the gene controlling basal bracts in QTL 1b* might also promote more cauline branches. Second, two transgressive, partially penetrant phenotypes appeared in the RILs: the bract position often shifted to a mid-peduncle position (**Fig. S11, A-F**) and signs of incomplete floral determinism (mostly branched flowers) were observed (**Fig. S11, N, O**). The shifted bract position resembles flower-preceding prophylls in some natural species (Endress 2006; Prenner et al. 2009). Interestingly, this phenotype is frequent in certain bract mutants like *soc1*, *tfl1* and even systematic in *bop1 x bop2* (**Fig. S11 H-M**). However, this trait did not correlate with any specific allelic combinations among the HIF families (**Fig. S11G**). Indeterminism in HIF 488 was associated with *Tsu-0* QTL 1b* and *Col-0* haplotypes in other mapped QTLs (**Fig. S11P**). Other indeterminism cases occurred in HIF 334, but without consistent genetic combinations of

mapped QTLs. Such transgressions suggest that complex genetic interactions may be required in *Tsu-0* to ensure proper bract development and positioning with a wild-type flower. To conclude, our data demonstrate that the genetic control of basal bracts in *Tsu-0* is complex and relies on several genes having additive effects on bract development and epistasis on other traits.

Transcriptomics of the floral transition suggests new pathways associated with bract development

To identify genes whose expression changes with bract development, we profiled meristem transcriptomes over the floral transition in both accessions. Microdissected meristems were matched to the same four developmental stages: vegetative, late vegetative, transition and floral (V, L, T and F, respectively, **Fig. 5A**). This ensured that, despite different absolute flowering times (**Fig. S12A**), the transcriptomes of the two accessions were realigned using the floral transition as a common developmental clock. After RNAseq, principal component analysis (PCA) validated replicate consistency (**Fig. S12B**) and the precision of the staging was confirmed by the synchronised expression between accessions of genes such as *FT*, *LFY* or *AP1*, key regulators of floral transition and flower identity (**Fig. 5B,** see also **Fig. S12C** for other reference genes). For LFY, this RNAseq data supported our results from the pLFY transcriptional reporter lines (**Fig. 2**) and genetic studies (**Fig. S4**), indicating that *LFY* is not involved in *Tsu-0* basal bract development. The stage T stood out as a critical transition, with the highest number of gene expression changes in both accessions (**Fig. 5C**). At stage T, *Col-0* and *Tsu-0* meristem transcriptomes also diverged the most, with up to 4,759 genes differentially expressed (DE) (**Fig. 5D**). Bract and flower initiations start before any morphological event (Heisler et al. 2005). Given the delay between stages T and F (a median of 1 to 2 days, **Fig. S12A**) and the plastochron (**Fig. 3B, C**), the first flowers and their bracts must be initiated at stage T. Thus, transcriptional changes associated with bract formation in *Tsu-0* should transiently appear at stage T and progressively fade by stage F since only the 1 to 5 first flowers present a bract (**Fig. 1C**, **Fig. S4H**).

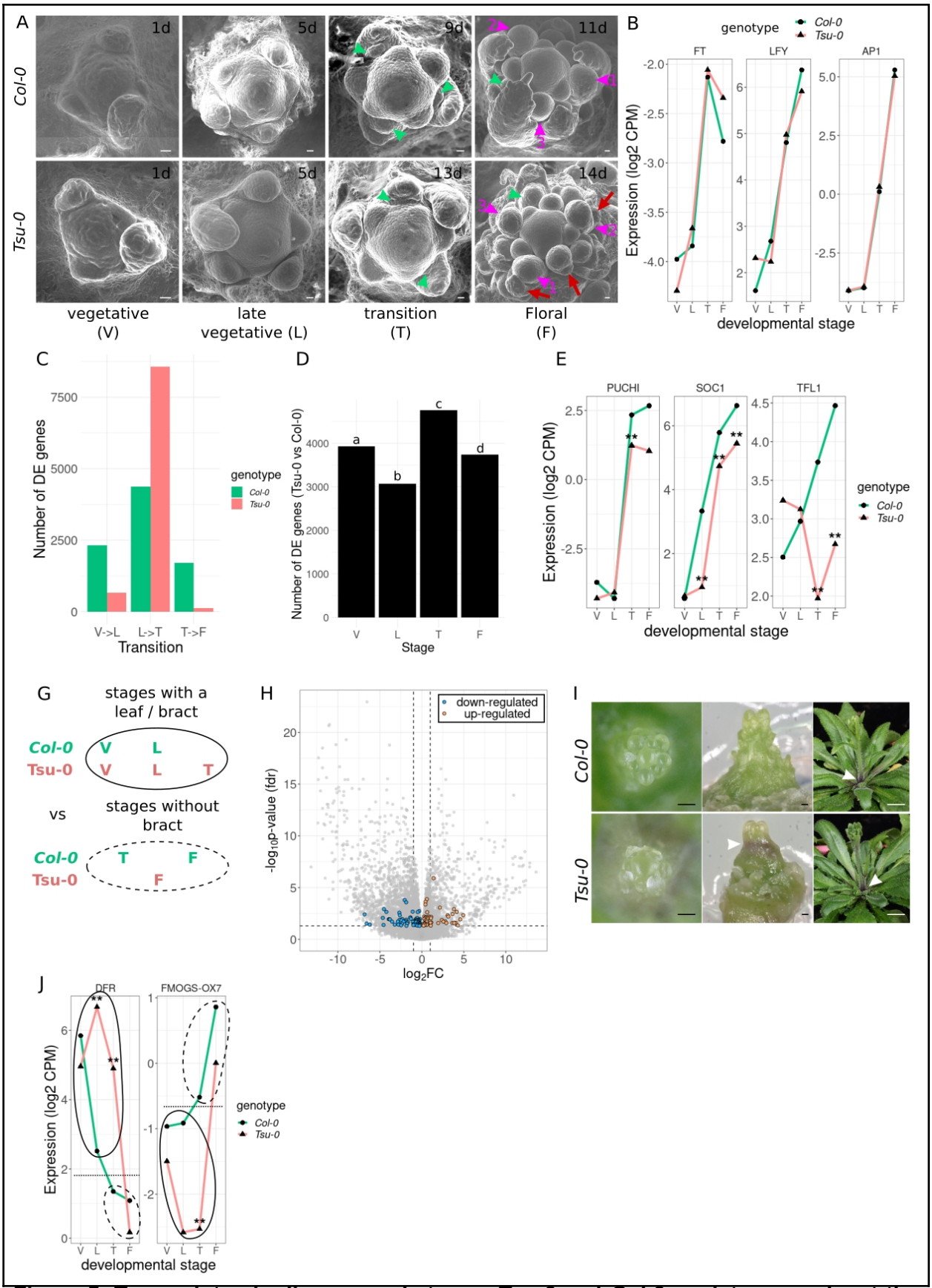

Figure 5: **Transcriptomic divergence between *Tsu-0* and *Col-0* meristems peaks at the**

Since GO terms yielded no informative clues from the high number of DE genes at stage T (**Fig. S14A**), we first examined whether known bract-related genes could be affected, although we knew from our mapping that they cannot be at the origin of basal bracts in *Tsu-0* (**Fig. 4I**). Only *PUCHI*, *SOC1* and *TFL1* significantly differed at stage T between *Tsu-0* and *Col-0* (**Fig. 5E** and **Fig. S12D**) but these differences persisted until stage F even though bracts disappeared with older flowers, suggesting that the variation of these gene expressions is not essential in bract formation.

To discover genes without *a priori*, we then performed a comparative transcriptomic approach with additional mutant data. Since *lfy* and *puchi x bop1 x bop2* mutants stop making leaves at floral transitions (I* branches, **Fig. S4B, D**) while *jagged-5d* plants always produce a bract, transcriptomic cues for bract development may only be present in *jagged-5d* meristems and not in the other two backgrounds. As expected from their genetic background and developmental stage, these mutants clustered with *Col-0* stage F in a PCA (**Fig. S12B**). By comparing DE genes of each mutant with *Col-0*, DE genes specific to jagged-5d were isolated (**Fig. S13A**). This set revealed an enrichment for biological processes related to shoot, phyllome development and photosynthesis, possibly linked to persistent bract formation (**Fig. S13B**). Only 413 of these genes were shared with DE genes of *Tsu-0* at stage T, with Go terms pointing again to chloroplast functions and less expectedly, to metal ion transport and homeostasis (**Fig. S13C, D**). If one of the causative genes mapped in *Tsu-0* (**Fig. 4, Table S1**) was differentially expressed (so not an allele acting post-transcriptionally) and shared with *jagged-5d*, it should be contained in this short list. Cross referencing transcriptomic and QTL-mapping datasets yielded 33 candidate genes (**Fig. S13E, Table S2**). None of them is known to be linked with bract development or with flowering in general. Although these particular genes should be validated, this mutant comparison suggests that new uncharacterized genetic pathways may be involved in the development of bracts.

In a third approach to capture genes involved in bract formation, we specifically took advantage of the time-series information. Briefly, expression data were gathered in two groups corresponding to either bract-less (*Col-0* T, F, and *Tsu-0* F) or leaf/bract-producing meristems (the other samples, including *Tsu-0* T) and we selected genes whose expression profile clusters

these two groups apart (**Fig. 5G**). Only 124 genes met the criteria of such "putative bract regulators" (**Fig. 5H, Table S3**), including *SOC1*, as a putative negative regulator. Just 19 genes overlapped with the genes also DE in *jagged-5d* (**Fig. S13C, Table S3**), without pointing to particular biological functions. Instead, two enriched GO-terms emerged from these putative bract regulators: anthocyanin biosynthesis and salicylic acid (SA), associated with up- and down-regulated genes, respectively (**Fig. S14D-F**). Backtracking these ontology terms for all DE genes at stage T (**Table S4** and **S5**) retrieved more genes associated with these pathways, supporting that their activity levels differ between *Tsu-0* and *Col-0* at the critical stage T (**Fig. S14I**). High anthocyanin production in *Tsu-0* at stages L and T was evident from the frequent purple coloration just below the meristems, contrasting with the green tissues in *Col-0* (**Fig. 5I**). Sometimes, this purple extended to young organs where bracts are initiated (**Fig. 14J**). As the stem grew, the pigment receded to the rosette junction in both accessions (**Fig. 5I**). This transient anthocyanin presence specific to *Tsu-0* supported our clustering strategy for capturing genes involved in transient bract development during flowering transition. Interestingly, among the 124 expression-based putative bract regulators (**Fig. 5H**), 12 also lied in the mapped QTLs (**Fig. 4I**). They all differed from the 33 genes selected before via specific overlap with *jagged-5d* (**Table S2**). Interestingly, we found one anthocyanin biosynthetic enzyme (the dihydroflavonol reductase, DFR) and five SA-responding genes (see **Table S3**). For example, **Figure 5J** shows the expression profiles of two such genes. Further work is required to test whether these candidates contribute to basal bract formation in *Tsu-0* and if the anthocyanin and/or SA pathways are involved in this natural variation. However, our transcriptomics exclude most of the genes previously associated with bract development in mutants, and suggest instead new candidate pathways promoting bract outgrowth with a wild-type flower during floral transition.

Bract development occurs in a time window when many genes are desynchronized

Our clustering approach (**Fig. 5G**) tended to select genes whose transcriptional dynamics were delayed in *Tsu-0* compared to *Col-0* (**Figure 5J**), with changes of RNA levels occurring later in *Tsu-0*. This defines a transcriptional heterochrony. Since bracts have been sometimes considered as a heterochrony because the juvenile leaf trait is maintained at older stages, we decided to characterise the extent of changes in the timing of gene expression between the two

accessions. We first plotted the two main axes of variance from a PCA after grouping samples by genotype and time points (**Fig. 6A**). While the second axis of variance (~24.4%) differentiates genotypes, the main axis (47.9% of variance) orders the sampling time points chronologically in both genotypes, representing a transcriptomic age. Surprisingly, *Tsu-0* stage T does not align with *Col-0* stage T on this axis, clustering instead with the stages F: this transcriptome is closer to a stage F, explaining the limited expression changes when progressing to the next stage F (**Fig. 5C**).

As suggested by (Calderwood et al. 2021), the transcriptomes of two genotypes during flowering cannot be aligned to a single developmental time; each gene may desynchronize differently, sometimes in opposite directions. To quantify gene desynchronization between *Col-0* and *Tsu-0*, we leveraged our previous approach of curve registration (Calderwood et al. 2021) to predict subtle temporal shifts of gene expression in our dataset (Kristianingsih 2024). This shift is relative to the floral transition, used as the common reference clock between the two accessions. Thus, genes with no shift, like *AP1* (**Fig. 5B and Fig. 6B**), may still be shifted in absolute time, because *Tsu-0* plants flower later with an older absolute age. Positive and negative shifts reflect desynchronization relative to the event of floral transition: gene expression dynamics may shift earlier or later. Unlike our previous clustering approach, this registration method uses a common scaled expression level and computes only temporal shifts, regardless of absolute expression levels (**Fig. 6B** and **Fig. S15A**). Few genes could not be registered (**Fig. 6B,** N = 43), suggesting that most genes follow similar temporal dynamics in both accessions (see examples **Fig. S12C, D** or **Fig. 5B, E**). Most genes were classified into three categories: null, negative and positive shifts (**Fig. 6B)**. A null shift indicates that the gene expression in *Tsu-0* stays “in phase” with flowering, like *AP1* (compared with **Fig. 5B)**. A positive

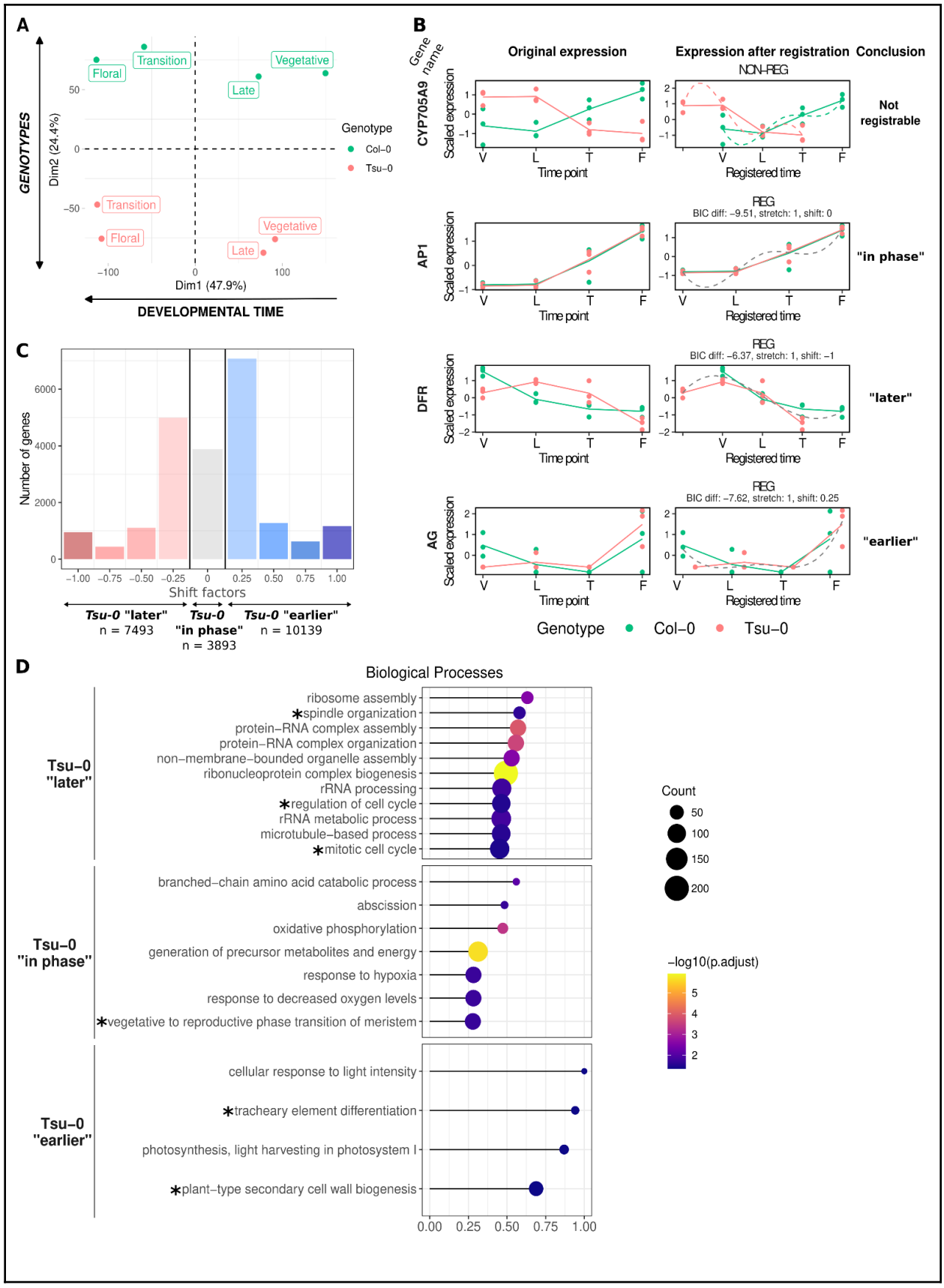

Figure 6: **Massive and complex transcriptional desynchronisation coexist in *Tsu-0* across the floral transition.**
A, PCA of RNAseq data from microdissected meristems of *Col-0* and *Tsu-0* over the four sampled stages (biological replicates averaged per time points). The two main axes of the PCA can be interpreted as developmental time and genotype, respectively.
B, Examples of temporal registration of gene dynamics (right panels) between *Col-0* (green) and *Tsu-0* (red) from scaled expression levels (left panel). Dots represent the expression levels of independent biological replicates, while lines indicate the mean expression level at each time point. In the right panel, the green (or red) dotted curves represent the fitted models for *Col-0* (or *Tsu-0*) independently, while the grey dotted curve represents the joint model for both *Col-0* and *Tsu-0*. If the green and red dotted curves are used, it means the two time series are best explained by two independent models, indicating they are not similar. Conversely, if the grey dotted curve is used, it suggests that a single model best explains both time series, indicating they are similar. The name of the gene plotted is indicated on the left of each row. These four genes exemplify the four possible categories (from top to bottom, respectively): genes that cannot be registered (N = 43, *e.g. CYP705A9*), genes with identical temporal dynamics (shift = 0, *e.g. AP1,* see also Fig. 5B) and genes whose expression dynamics in *Tsu-0* must be shifted negatively (*e.g. DFR,* see also Fig. 5J) or positively (*e.g. AG*) to align with *Col-0*. The last column provides a biological interpretation of the computed shift (see main text): a null shift indicates that the expression dynamics in *Tsu-0* stay "*in phase*" with floral transition while negative or positive shifts indicate that the expression dynamics in *Tsu-0* are desynchronized later or earlier, respectively, than the phenotypic progression of floral transition.
C, Distribution of heterochronic shifts between *Tsu-0* and *Col-0* on the entire meristematic transcriptome, computed by the registration method from B. The shift value is colour-coded in a red-to-blue gradient from -1 to 1.
D, GO term enrichment analysis associated with the three categories of heterochronic shifts. The list of all significant 'biological process' GO terms (BH-adjusted p.value < 0.05) was simplified using semantic similarity (cutoff = 0.7) and the Rich Factor was computed for the remaining terms, revealing the proportion of genes involved among all the genes associated with this GO term. Dot size indicates the count of genes and the color scale is the statistical significance (BH-adjusted p.value) of the enrichment in the shift category. Stars indicate GO terms referring to developmental processes.

or negative shift indicates that gene dynamics in *Tsu-0* occur earlier *(e.g. AG*) or later (*e.g.*, *DFR*, see also **Fig. 5J**), relative to the floral transition, revealing heterochronies between transcriptomic and phenotypic processes. Transcriptome-wide, the shifts were broadly distributed, showing massive and complex desynchronisation of gene dynamics (**Fig. 6C**). The floral transition in Tsu-0 did not impose its clock to the entire meristematic transcriptome: only ~18% of genes (n=3879) stayed in phase with this process while the majority showed delayed or advanced expression dynamics. Even more genes shifted earlier relative to the floral transition,

supporting the PCA interpretation (**Fig. 6A**) and confirming that the bract, if considered as "juvenile", did not represent the majority of heterochronies at the transcriptomic level.

As expected, genes in phase were primarily linked to flowering and developmental phase change as shown by key regulators of these pathways (**Fig. S15B, C**), which also emerges from GO term enrichment analysis (**Fig. 6D**). In contrast, known bract genes exhibit a wide range of shifts, from very early to very late, suggesting that they are not collectively involved in *Tsu-0* bract development (**Fig. S15A, C**). GO term analysis for each shift category highlighted the particular processes desynchronized from flowering in *Tsu-0* compared to *Col-0* (**Fig. 6D**). For instance, vascular differentiation (two GO terms mentioning tracheary element and secondary cell wall) emerges as a process shifted earlier in *Tsu-0* relative to the floral transition **(Fig. 6D)**. Its dynamics may be driven by other progression factors like absolute age, suggesting its loose connection with the flowering pathway. Conversely, processes shifted later in *Tsu-0* revealed terms related to cell division (spindle, cell cycle, mitosis) and ribosomal biogenesis (six GO terms mentioning ribosome, rRNA, ribonucleoprotein and protein-RNA complexes; **Fig. 6D**), which suggests that core meristematic functions are prolonged in *Tsu-0*. Further work is yet needed to explore whether the desynchronization of these processes relative to floral transition impacts bract development.

Finally, this focus on gene desynchronisation provided an explanation to the fact that gene expression diverged most at the stage T (**Fig. 5D**). The genes controlling floral transition change swiftly their expression levels upon stage T when many other genes have different levels between both accessions, because they are no longer synchronised with flowering in *Tsu-0* (**Fig. S16**). A transient process such as flowering is likely to occur in varying gene expression states, especially if it is fast and depends on a small number of genes. Massive desynchronization of gene dynamics creates transcriptional variation, potentially leading to developmental variation at the time of flowering, such as bract development. In conclusion, our work provides the first analysis of transcriptome-wide meristematic heterochronies between two *A. thaliana* accessions, revealing that natural bract development during floral transition is more complex than a prolonged vegetative phase.

Discussion

This study documents a natural variation for the presence of bracts at the base of flowering branches in *A. thaliana*, which was used to investigate their genetic and developmental basis. Comprehensive phenotypic characterizations indicate strong differences with known mutant bracts and similarities with bracts of bracteate species. Combining quantitative genetics, genomics and meristem transcriptomics on the accession *Tsu-0*, our results suggest new mechanisms controlling bract outgrowth and highlight the phenomenon of massive gene desynchronizations at floral transition, raising new questions about their implications in development and evolution.

A new mechanism unlocking bract development without affecting floral identity during floral transition

We used two quantitative genetics approaches (BSA and RIL) and a transcriptomic approach to identify the genetic mechanisms controlling basal bract formation in *Tsu-0*. We identified at least four major QTLs, the two main on chromosome 1 with additive effects (**Fig. 4** and **Fig. S7**). However, the density of polymorphisms between the two accessions and the high number of differentially expressed genes resulted in many potential candidates within the mapped intervals. Further fine-mapping or a GWAS analysis on a larger accession panel could provide a higher resolution and even reveal more causative variations.

Our work also proposes new pathways for bract development: genetic interactions between *SOC1*, *TFL1* and *PUCHI* (**Fig. 5E**), chloroplast or metal ion transport and homeostasis (**Fig. S13D**), anthocyanin biosynthesis and response to salicylic acid (**Fig. 5I, J**; **Fig. S14E-J**), ribosome biogenesis (**Fig. 6D**). The low number of transcription factors (**tables S1, S2, S3**) compared to enzymes and genes related to metabolic pathways (**Fig. 5 and 6**; **Fig. S13 and S14**) aligns with studies reporting that genes with basic metabolic and cellular functions control specific developmental processes in plants (Tsukaya et al. 2013). Likewise, the *PLA1/2/3* genes In *Poaceae* are three unrelated metabolic enzymes (a cytochrome P450, MEI2-like RNA-binding protein and a glutamate carboxypeptidase II, respectively) that partially suppress bract outgrowth in a redundant manner through a still unknown mechanism (Kawakatsu et al. 2009;

Wang et al. 2021). Our data may thus be helpful to investigate the mechanisms that control bract development.

Despite the remaining uncertainty about the causal genes and pathways, our data show the existence of a new bract developmental process different from regained bracts produced in mutants. *Tsu-0* basal bracts display specific features: association with wild-type flowers (**Fig. 2** and **Fig. S2, S3**); wild-type bract shape and position (**Fig. 1**, **Fig. S11**); presence restricted at the base of the raceme (**Fig. S4, S5**); no modification of plastochron rate (**Fig. 3B, Fig. S6A**); independence from light regime (**Fig. 3D**). Not only such phenotypes differ from those reported in bract mutants, but none of the known "bract mutant genes" were found in QTL intervals, indicating that the causal polymorphisms involve other genes and that bract development could be de-repressed without affecting floral meristem identity. However, because of the transgressive indeterminism observed in some RILs (**Fig. S11**), it cannot be ruled out that some of the bract causal genes could also affect flower development, but genetic interactions would suppress these floral phenotypes while maintaining the basal bracts.

Transcriptomic heterochronies at floral transition may challenge developmental canalization

The transient formation of bracts at the base of each raceme raises many biological questions. This trait is widespread within the *Brassicaceae* phylogeny (**Fig. 1S**). It is also known for decades that several species within their natural context display developmental variations at the base of the raceme, including bracts, flower-to-shoot transformations, or flower dimorphisms (Arber 1931a; Arber 1931b). Since these basal nodes are produced just at the floral transition, this suggests that developmental canalization (ensuring an invariant phenotypic output) is less effective at this stage. The variability of bract formation from branch to branch and plant to plant (**Fig. 1 D-F, Fig. 4A**) also suggests limited developmental canalization. Our data show that natural genetic variation is sufficient to reveal a higher frequency of phenotypic variations at the base of branches. To our knowledge, no specific hypothesis has been proposed to explain the lower developmental canalization at the floral transition.

We propose that transcriptional heterochronies may account for some of this phenomenon. In bract-less species, bract development is often described as a prolonged vegetative state,

728 characterised by the persistence of a juvenile trait (a leaf) with an adult trait (a flower)(Alberch
729 et al. 1979; Buendía-Monreal and Gillmor 2018). Using microdissected meristems at different
730 stages (**Fig. 5**), we expected to find this signature in the bract-making *Tsu-0* transcriptome.
731 Instead, we discovered that the floral transition occurs in an older transcriptome rather than a
732 younger one (**Fig. 6A, C**). In absolute time, *Tsu-0* plants flower later (**Fig. 3 E, F; Fig. S12 A**), so
733 the flowering-related genes are actually shifted later. However, a large majority of genes get
734 out of synchronisation with flowering. In absolute time, some may keep their dynamics or even
735 shift earlier, both categorised as "earlier" in our analysis using flowering as the reference, while
736 other genes can shift even later than flowering (**Fig. 6 B, C**). Confirming our previous results
737 using *Brassica rapa* cultivars and *A. thaliana* (Calderwood et al. 2021), such massive and
738 complex gene desynchronisation during floral transition seems to be a general rule at both
739 intra- and inter-species level. Flowering time is under strong selection pressure in *A. thaliana*
740 (Bloomer and Dean 2017). If selective adaptation of flowering time constantly shifts and
741 desynchronizes the flowering-related genes from numerous others, this can create new global
742 gene expression states, especially at the transition when gene expressions vary quickly (**Fig.**
743 **S16**). This could promote transient developmental variations, like basal bracts.
744 The consequence of gene desynchronization is to create a peak of transcriptome divergence
745 upon floral transition. Such a peak has been reported in *Solanaceae* where it was associated
746 with the phenotypic evolution of inflorescence complexity (Lemmon et al. 2016). Mirroring the
747 "inverse hourglass" model for animal embryogenesis, morphological variations would be
748 promoted by transcriptomic divergence during intermediate developmental steps. Hence, the
749 sensitivity of floral transition to heterochronies at the transcriptional level could have larger
750 implications for phenotypic evolution from populations to species.

751 ***Evolution of bract loss in Brassicaceae and Angiosperms and the possible role of***
752 ***heterochronies***

753 Heterochrony is often considered as a powerful mechanism for evolutionary change (Buendía-
754 Monreal and Gillmor 2018; Petrone-Mendoza et al. 2023). Here, we propose that
755 heterochronies at the floral transition may lower developmental canalization, contributing to
756 bract derepression in some accessions. Conversely, heterochronies might have been involved in

bract loss in the *Brassicaceae* ancestor. Current evolutionary scenarios for bract loss are deduced from mutants and do not involve heterochrony. In *A. thaliana*, flowers would have evolved the ability to repress bract development (Whipple et al. 2010), while In *Poaceae*, boundary regions may have acquired this function through genes like NTT (Whipple et al. 2010; Xiao et al. 2022). However, direct regulation of NTT by SPL genes in maize (Xiao et al. 2022) and rice (Wang et al. 2021) provide a link with a major regulator of heterochrony in plants, the SPL/miR156 balance (Buendía-Monreal and Gillmor 2018). SPL genes have not been found to control bract development in *A. thaliana*. Recently, *SOC1*, *FUL* and *AGL24* were shown to be more effective than *LFY* or *BOP1/2* in repressing bracts (Manuela and Xu 2024 Mar 28). These genes are special because they act both as FMI genes and as flowering time genes. Our data did not correlate bract outgrowth with any FMI genes (**Fig. 2, Fig. 5**) while flowering time was clearly impacted at the phenotypic (**Fig. 3E, F**) and transcriptional level (*e.g.*, *FLC* in **Fig. S12C or Fig. S15C**). Since flowering time is prone to heterochrony, this could connect bract with heterochrony in *A. thaliana*. Hence, despite differences in molecular players, bract outgrowth in *Brassicaceae* and *Poaceae* may share more similarities than previously described.

Deducing evolutionary events from mutants relies on the assumption that natural evolution proceeds in the opposite direction to artificial mutants, which should be taken with caution. Indeed, actual ebracteate plants have accumulated many evolutionary changes since they diverged from the last bracteate ancestor: genetic interactions revealed by mutants in current species may be totally irrelevant in the ancestor. It has also been proposed as the “Dollo’s law” (Gould 1970) that lost traits cannot be regained and “*must be constructed afresh in some different mode*” (Arber 1918). However, heterochronies have been proposed as a mechanism to break Dollo’s law (Cronk 2009). Since ebracteate plants still produce leaves elsewhere, activating or repressing this functional developmental program by heterochronies could effectively coordinate bract and flower development, explaining both bract loss and their “flickering presence” (Marshall et al. 1994) within and between species in the entire *Brassicaceae* family. Further work, notably including different bracteate and ebracteate species, will be necessary to test these hypotheses and clarify the genetic and developmental mechanisms that led to bract loss in *Brassicaceae*.

Acknowledgements

We thank Teva Vernoux for the critical reading of the manuscript. We thank Mathieu Hanemian, Gaël Yvert and Bjorn Pieper for their advice in quantitative genetics. We thank Thomas Widiez and Nathanaël Jacquier for their advice in Kasp genotyping. We thank Michiel Vandenbussche for providing the picture of a Petunia plant (Fig. 1A). We thank the following researchers for providing *A. thaliana* mutant seed stocks: Mitsuhiro Aida for *puchi-1*, *bop1-4* x *bop2-11*, and *puchi-1 x bop1-4 x bop2-11* ; Jiawei Wang for *soc1-2 x agl24-1 x svp-41* ; Hicham Chathane for *lfy-12* ; Georges Coupland and Enric Bertran Garcia de Olalla for *soc1-2*. We thank Pr Eric Schranz and Frank Becker, from Wageningen University (WUR, Holland) for providing seeds of *Tarenaya hassleriana* and *Gynandropis gynandra*. We acknowledge the PSMN (Pôle Scientifique de Modélisation Numérique) computing centre of 'ENS de Lyon' for providing support in the genomic variant analysis. We thank the Embassy of France in the United Kingdom for a short-term travel fellowship awarded to R. K. R.M. and R.W. gratefully acknowledge support from the Biotechnology and Biological Science Research Council Institute Strategic Programme ‘Building Resilience in Crops’ (BB/X01102X/1).

Competing interests,

The authors declare that they have no competing interests

Author contributions

Sana Dieudonné: Conceptualization, Investigation, Software (implementation), Formal analysis, Visualization, Methodology, Writing -review and editing; Ruth Kristianingsih: Formal Analysis, Methodology, Software (designing, programming, testing, implementing), Visualization, Writing -review and editing; Stephanie Laine, Investigation; Béline Jesson: Formal analysis, Véronique Vidal: Supervision, Rachel Wells: Supervision, Writing -review and editing; Richard Morris: Supervision, Writing -review and editing; Fabrice Besnard: Conceptualization, Project administration, Supervision, Investigation, Formal analysis, Methodology, Software (programming, implementing), Funding acquisition, Visualization, Writing - original draft, review and editing.

Data availability

Whole-genome DNA-seq data of the parental lines (*Col-0* and *Tsu-0*) and of the two F2 pools used for bulk segregant analysis are deposited under this identifier: doi:10.57745/Z80SIM. Time-course RNA-seq data of *Col-0* and *Tsu-0* micro-dissected meristems during flowering are available with these doi: doi:10.57745/DKMQ06, doi:10.57745/7JI3E7, respectively. RNA-seq data of micro-dissected shoot meristems of the mutant lines (*puchi-1x bop1-4* x *bop2-11*, *lfy-12* and *jagged-5d)* at early flowering stage are available at doi:10.57745/HAGJJH.

References

Alberch P, Gould SJ, Oster GF, Wake DB. 1979. Size and Shape in Ontogeny and Phylogeny. Paleobiology. 5(3):296–317.

Al-Shehbaz IA. 2015. Cardamine xinfenii (Brassicaceae), a New Species from Sichuan (China). Harvard Papers in Botany. 20(2):145–146.

Anders S, Huber W. 2010. Differential expression analysis for sequence count data. Genome Biol. 11(10):R106. doi:10.1186/gb-2010-11-10-r106.

Arber A. 1918. The “Law of Loss” in Evolution. Proc Linn Soc Lond. 131:70–78.

Arber A. 1931a. Studies in Floral Morphology. I. On Some Structural Features of the Cruciferous Flower. The New Phytologist. 30(1):11–41.

Arber A. 1931b. Studies in Floral Morphology. II. Some Normal and Abnormal Crucifers: with a Discussion on teratology and Atavism. The New Phytologist. 30(3):172–203.

Balanzà V, Martínez-Fernández I, Ferrándiz C. 2014. Sequential action of FRUITFULL as a modulator of the activity of the floral regulators SVP and SOC1. J Exp Bot. 65(4):1193–1203. doi:10.1093/jxb/ert482.

van Berloo R. 2008. GGT 2.0: Versatile Software for Visualization and Analysis of Genetic Data. Journal of Heredity. 99(2):232–236. doi:10.1093/jhered/esm109.

Besnard F, Picao-Osorio J, Dubois C, Félix M-A. 2020. A broad mutational target explains a fast rate of phenotypic evolution. Weigel D, Landry CR, Matus D, editors. eLife. 9:e54928. doi:10.7554/eLife.54928.

Bloomer RH, Dean C. 2017. Fine-tuning timing: natural variation informs the mechanistic basis of the switch to flowering in Arabidopsis thaliana. Journal of Experimental Botany.

68(20):5439–5452. doi:10.1093/jxb/erx270.

Bolger AM, Lohse M, Usadel B. 2014. Trimmomatic: a flexible trimmer for Illumina sequence data. Bioinformatics. 30(15):2114–2120. doi:10.1093/bioinformatics/btu170.

Bowman JL, Alvarez J, Weigel D, Meyerowitz EM, Smyth DR. 1993. Control of flower development in Arabidopsis thaliana by APETALA1 and interacting genes. Development. 119(3):721–743. doi:10.1242/dev.119.3.721.

Broman KW, Gatti DM, Simecek P, Furlotte NA, Prins P, Sen Ś, Yandell BS, Churchill GA. 2019. R/qtl2: Software for Mapping Quantitative Trait Loci with High-Dimensional Data and Multiparent Populations. Genetics. 211(2):495–502. doi:10.1534/genetics.118.301595.

Buendía-Monreal M, Gillmor CS. 2018. The times they are a-changin': heterochrony in plant development and evolution. Frontiers in Plant Science. 9. doi:10.3389/fpls.2018.01349.

Calderwood A, Hepworth J, Woodhouse S, Bilham L, Jones DM, Tudor E, Ali M, Dean C, Wells R, Irwin JA, et al. 2021. Comparative transcriptomics reveals desynchronisation of gene expression during the floral transition between Arabidopsis and Brassica rapa cultivars. Quant Plant Biol. 2:e4. doi:10.1017/qpb.2021.6.

Carlson M. 2024. org.At.tair.db: Genome wide annotation for Arabidopsis.

Chahtane H, Zhang B, Norberg M, LeMasson M, Thévenon E, Bakó L, Benlloch R, Holmlund M, Parcy F, Nilsson O, et al. 2018. LEAFY activity is post-transcriptionally regulated by BLADE ON PETIOLE2 and CULLIN3 in Arabidopsis. New Phytol. 220(2):579–592. doi:10.1111/nph.15329.

Chen Y, Lun ATL, Smyth GK. 2016. From reads to genes to pathways: differential expression analysis of RNA-Seq experiments using Rsubread and the edgeR quasi-likelihood pipeline. doi:10.12688/f1000research.8987.2. [accessed 2024 Jul 16]. https://f1000research.com/articles/5-1438.

Cheng C-Y, Krishnakumar V, Chan AP, Thibaud-Nissen F, Schobel S, Town CD. 2017. Araport11: a complete reannotation of the Arabidopsis thaliana reference genome. Plant J. 89(4):789–804. doi:10.1111/tpj.13415.

Chuck G, Cigan AM, Saeteurn K, Hake S. 2007. The heterochronic maize mutant Corngrass1 results from overexpression of a tandem microRNA. Nat Genet. 39(4):544–549.

873 doi:10.1038/ng2001.
874 Chuck G, Whipple C, Jackson D, Hake S. 2010. The maize SBP-box transcription factor encoded
875 by tasselsheath4 regulates bract development and the establishment of meristem
876 boundaries. Development. 137(8):1243–1250. doi:10.1242/dev.048348.
877 Chuck GS, Brown PJ, Meeley R, Hake S. 2014. Maize SBP-box transcription factors unbranched2
878 and unbranched3 affect yield traits by regulating the rate of lateral primordia initiation.
879 Proc Natl Acad Sci U S A. 111(52):18775–18780. doi:10.1073/pnas.1407401112.
880 Cingolani P, Platts A, Wang LL, Coon M, Nguyen T, Wang L, Land SJ, Lu X, Ruden DM. 2012. A
881 program for annotating and predicting the effects of single nucleotide polymorphisms,
882 SnpEff: SNPs in the genome of Drosophila melanogaster strain w1118; iso-2; iso-3. Fly
883 (Austin). 6(2):80–92. doi:10.4161/fly.19695.
884 Clough SJ, Bent AF. 1998. Floral dip: a simplified method for Agrobacterium-mediated
885 transformation of Arabidopsis thaliana. Plant J. 16(6):735–743.
886 Cronk QCB. 2009. Evolution in reverse gear: the molecular basis of loss and reversal. Cold Spring
887 Harb Symp Quant Biol. 74:259–266. doi:10.1101/sqb.2009.74.034.
888 Cutler SR, Ehrhardt DW, Griffitts JS, Somerville CR. 2000. Random GFP::cDNA fusions enable
889 visualization of subcellular structures in cells of Arabidopsis at a high frequency. Proc
890 Natl Acad Sci U S A. 97(7):3718–3723. doi:10.1073/pnas.97.7.3718.
891 Dinneny JR, Yadegari R, Fischer RL, Yanofsky MF, Weigel D. 2004. The role of JAGGED in shaping
892 lateral organs. Development. 131(5):1101–1110. doi:10.1242/dev.00949.
893 Dobin A, Davis CA, Schlesinger F, Drenkow J, Zaleski C, Jha S, Batut P, Chaisson M, Gingeras TR.
894 2013. STAR: ultrafast universal RNA-seq aligner. Bioinformatics. 29(1):15–21.
895 doi:10.1093/bioinformatics/bts635.
896 Endress PK. 2006. Angiosperm Floral Evolution: Morphological Developmental Framework. In:
897 Advances in Botanical Research. Vol. 44. Academic Press. (Developmental Genetics of
898 the Flower). p. 1–61. [accessed 2023 Dec 1].
899 https://www.sciencedirect.com/science/article/pii/S0065229606440015.
900 Garnier, Simon, Ross, Noam, Rudis, Robert, Camargo, Pedro A, Sciaini, Marco, et al. 2024.
901 viridis(Lite) - Colorblind-Friendly Color Maps for R. https://sjmgarnier.github.io/viridis/.

902 German DA, Hendriks KP, Koch MA, Lens F, Lysak MA, Bailey CD, Mummenhoff K, Al-Shehbaz IA.
903 2023. An updated classification of the Brassicaceae (Cruciferae). PhytoKeys. 220:127–
904 144. doi:10.3897/phytokeys.220.97724.
905 Goldshmidt A, Alvarez JP, Bowman JL, Eshed Y. 2008. Signals derived from YABBY gene activities
906 in organ primordia regulate growth and partitioning of Arabidopsis shoot apical
907 meristems. Plant Cell. 20(5):1217–1230. doi:10.1105/tpc.107.057877.
908 Gould SJ. 1970. Dollo on Dollo's Law: Irreversibility and the Status of Evolutionary Laws. Journal
909 of the History of Biology. 3(2):189–212.
910 Grandi V, Gregis V, Kater MM. 2012. Uncovering genetic and molecular interactions among
911 floral meristem identity genes in Arabidopsis thaliana. Plant J. 69(5):881–893.
912 doi:10.1111/j.1365-313X.2011.04840.x.
913 Healey A, Furtado A, Cooper T, Henry RJ. 2014. Protocol: a simple method for extracting next-
914 generation sequencing quality genomic DNA from recalcitrant plant species. Plant
915 Methods. 10:21. doi:10.1186/1746-4811-10-21.
916 Heisler MG, Ohno C, Das P, Sieber P, Reddy GV, Long JA, Meyerowitz EM. 2005. Patterns of
917 auxin transport and gene expression during primordium development revealed by live
918 imaging of the Arabidopsis inflorescence meristem. Curr Biol. 15(21):1899–1911.
919 doi:10.1016/j.cub.2005.09.052.
920 Helsen J, Voordeckers K, Vanderwaeren L, Santermans T, Tsontaki M, Verstrepen KJ, Jelier R.
921 2020. Gene Loss Predictably Drives Evolutionary Adaptation. Mol Biol Evol. 37(10):2989–
922 3002. doi:10.1093/molbev/msaa172.
923 Hempel FD, Feldman LJ. 1995. Specification of chimeric flowering shoots in wild-type
924 Arabidopsis. Plant J. 8(5):725–731. doi:10.1046/j.1365-313x.1995.08050725.x.
925 Hempel FD, Zambryski PC, Feldman LJ. 1998. Photoinduction of flower identity in vegetatively
926 biased primordia. Plant Cell. 10(10):1663–1676. doi:10.1105/tpc.10.10.1663.
927 Hepworth SR, Klenz JE, Haughn GW. 2006. UFO in the Arabidopsis inflorescence apex is
928 required for floral-meristem identity and bract suppression. Planta. 223(4):769–778.
929 doi:10.1007/s00425-005-0138-3.
930 Hepworth SR, Zhang Y, McKim S, Li X, Haughn GW. 2005. BLADE-ON-PETIOLE-dependent

signaling controls leaf and floral patterning in Arabidopsis. Plant Cell. 17(5):1434–1448. doi:10.1105/tpc.104.030536.

Houston K, Druka A, Bonar N, Macaulay M, Lundqvist U, Franckowiak J, Morgante M, Stein N, Waugh R. 2012. Analysis of the barley bract suppression gene Trd1. Theor Appl Genet. 125(1):33–45. doi:10.1007/s00122-012-1814-x.

Huber W, Carey VJ, Gentleman R, Anders S, Carlson M, Carvalho BS, Bravo HC, Davis S, Gatto L, Girke T, et al. 2015. Orchestrating high-throughput genomic analysis with Bioconductor. Nat Methods. 12(2):115–121. doi:10.1038/nmeth.3252.

Irish VF, Sussex IM. 1990. Function of the apetala-1 gene during Arabidopsis floral development. Plant Cell. 2(8):741–753. doi:10.1105/tpc.2.8.741.

Itoh JI, Hasegawa A, Kitano H, Nagato Y. 1998. A recessive heterochronic mutation, plastochron1, shortens the plastochron and elongates the vegetative phase in rice. Plant Cell. 10(9):1511–1522. doi:10.1105/tpc.10.9.1511.

Karim MR, Hirota A, Kwiatkowska D, Tasaka M, Aida M. 2009. A role for Arabidopsis PUCHI in floral meristem identity and bract suppression. Plant Cell. 21(5):1360–1372. doi:10.1105/tpc.109.067025.

Kawakatsu T, Itoh J-I, Miyoshi K, Kurata N, Alvarez N, Veit B, Nagato Y. 2006. PLASTOCHRON2 regulates leaf initiation and maturation in rice. Plant Cell. 18(3):612–625. doi:10.1105/tpc.105.037622.

Kawakatsu T, Taramino G, Itoh J-I, Allen J, Sato Y, Hong S-K, Yule R, Nagasawa N, Kojima M, Kusaba M, et al. 2009. PLASTOCHRON3/GOLIATH encodes a glutamate carboxypeptidase required for proper development in rice. Plant J. 58(6):1028–1040. doi:10.1111/j.1365-313X.2009.03841.x.

Kiefer M, Schmickl R, German DA, Mandáková T, Lysak MA, Al-Shehbaz IA, Franzke A, Mummenhoff K, Stamatakis A, Koch MA. 2014. BrassiBase: introduction to a novel knowledge database on Brassicaceae evolution. Plant Cell Physiol. 55(1):e3. doi:10.1093/pcp/pct158.

Kinoshita A, Vayssières A, Richter R, Sang Q, Roggen A, van Driel AD, Smith RS, Coupland G. 2020. Regulation of shoot meristem shape by photoperiodic signaling and

phytohormones during floral induction of Arabidopsis. Elife. 9:e60661. doi:10.7554/eLife.60661.

Kristianingsih R. 2024. greatR: Gene Registration from Expression and Time-Courses in R. https://ruthkr.github.io/greatR/.

Kwiatkowska D. 2006. Flower primordium formation at the Arabidopsis shoot apex: quantitative analysis of surface geometry and growth. J Exp Bot. 57(3):571–580. doi:10.1093/jxb/erj042.

Kwiatkowska D. 2008. Flowering and apical meristem growth dynamics. J Exp Bot. 59(2):187–201. doi:10.1093/jxb/erm290.

Lawrence M, Gentleman R, Carey V. 2009. rtracklayer: an R package for interfacing with genome browsers. Bioinformatics. 25(14):1841–1842. doi:10.1093/bioinformatics/btp328.

Lawrence M, Huber W, Pagès H, Aboyoun P, Carlson M, Gentleman R, Morgan MT, Carey VJ. 2013. Software for computing and annotating genomic ranges. PLoS Comput Biol. 9(8):e1003118. doi:10.1371/journal.pcbi.1003118.

Lemmon ZH, Park SJ, Jiang K, Van Eck J, Schatz MC, Lippman ZB. 2016. The evolution of inflorescence diversity in the nightshades and heterochrony during meristem maturation. Genome Res. 26(12):1676–1686. doi:10.1101/gr.207837.116.

Levin JZ, Meyerowitz EM. 1995. UFO: an Arabidopsis gene involved in both floral meristem and floral organ development. Plant Cell. 7(5):529–548. doi:10.1105/tpc.7.5.529.

Liu C, Xi W, Shen L, Tan C, Yu H. 2009. Regulation of floral patterning by flowering time genes. Dev Cell. 16(5):711–722. doi:10.1016/j.devcel.2009.03.011.

Long J, Barton MK. 2000. Initiation of axillary and floral meristems in Arabidopsis. Dev Biol. 218(2):341–353. doi:10.1006/dbio.1999.9572.

Love MI, Huber W, Anders S. 2014. Moderated estimation of fold change and dispersion for RNA-seq data with DESeq2. Genome Biol. 15(12):550. doi:10.1186/s13059-014-0550-8.

Maizel A, Weigel D. 2004. Temporally and spatially controlled induction of gene expression in Arabidopsis thaliana. The Plant Journal. 38(1):164–171. doi:10.1111/j.1365-313X.2004.02027.x.

989 Mansfeld BN, Grumet R. 2018. QTLseqr: An R Package for Bulk Segregant Analysis with Next-
990 Generation Sequencing. Plant Genome. 11(2). doi:10.3835/plantgenome2018.01.0006.
991 Manuela D, Xu M. 2024 Mar 28. Aintegumenta And Redundant Aintegumenta-Like6 Are
992 Required For Bract Outgrowth In Arabidopsis. J Exp Bot.:erae138.
993 doi:10.1093/jxb/erae138.
994 Marshall CR, Raff EC, Raff RA. 1994. Dollo's law and the death and resurrection of genes. Proc
995 Natl Acad Sci U S A. 91(25):12283–12287. doi:10.1073/pnas.91.25.12283.
996 McCarthy DJ, Chen Y, Smyth GK. 2012. Differential expression analysis of multifactor RNA-Seq
997 experiments with respect to biological variation. Nucleic Acids Res. 40(10):4288–4297.
998 doi:10.1093/nar/gks042.
999 Melzer S, Lens F, Gennen J, Vanneste S, Rohde A, Beeckman T. 2008. Flowering-time genes
1000 modulate meristem determinacy and growth form in Arabidopsis thaliana. Nat Genet.
1001 40(12):1489–1492. doi:10.1038/ng.253.
1002 Michaels SD, Ditta G, Gustafson-Brown C, Pelaz S, Yanofsky M, Amasino RM. 2003. AGL24 acts
1003 as a promoter of flowering in Arabidopsis and is positively regulated by vernalization.
1004 The Plant Journal. 33(5):867–874. doi:10.1046/j.1365-313X.2003.01671.x.
1005 Miyoshi K, Ahn B-O, Kawakatsu T, Ito Y, Itoh J-I, Nagato Y, Kurata N. 2004. PLASTOCHRON1, a
1006 timekeeper of leaf initiation in rice, encodes cytochrome P450. Proc Natl Acad Sci U S A.
1007 101(3):875–880. doi:10.1073/pnas.2636936100.
1008 Nilsson O, Wu E, Wolfe DS, Weigel D. 1998. Genetic ablation of flowers in transgenic
1009 Arabidopsis. Plant J. 15(6):799–804. doi:10.1046/j.1365-313x.1998.00260.x.
1010 Norberg M, Holmlund M, Nilsson O. 2005. The BLADE ON PETIOLE genes act redundantly to
1011 control the growth and development of lateral organs. Development. 132(9):2203–
1012 2213. doi:10.1242/dev.01815.
1013 Ohno CK, Reddy GV, Heisler MGB, Meyerowitz EM. 2004. The Arabidopsis JAGGED gene
1014 encodes a zinc finger protein that promotes leaf tissue development. Development.
1015 131(5):1111–1122. doi:10.1242/dev.00991.
1016 Pasha A, Subramaniam S, Cleary A, Chen X, Berardini T, Farmer A, Town C, Provart N. 2020.
1017 Araport Lives: An Updated Framework for Arabidopsis Bioinformatics. Plant Cell.

32(9):2683–2686. doi:10.1105/tpc.20.00358.

Penin AA. 2008. Bract reduction in Cruciferae: possible genetic mechanisms and evolution. Wulfenia. 15:63–73.

Petrone-Mendoza E, Vergara-Silva F, Olson ME. 2023. Plant morpho evo-devo. Trends Plant Sci. 28(11):1257–1276. doi:10.1016/j.tplants.2023.06.007.

Prenner G, Vergara-Silva F, Rudall PJ. 2009. The key role of morphology in modelling inflorescence architecture. Trends Plant Sci. 14(6):302–309. doi:10.1016/j.tplants.2009.03.004.

R Core Team. 2018. R: A Language and Environment for Statistical Computing. R Foundation for Statistical Computing. Vienna, Austria. https://www.R-project.org/.

Ratcliffe OJ, Amaya I, Vincent CA, Rothstein S, Carpenter R, Coen ES, Bradley DJ. 1998. A common mechanism controls the life cycle and architecture of plants. Development. 125(9):1609–1615. doi:10.1242/dev.125.9.1609.

Ritchie ME, Phipson B, Wu D, Hu Y, Law CW, Shi W, Smyth GK. 2015. limma powers differential expression analyses for RNA-sequencing and microarray studies. Nucleic Acids Research. 43(7):e47. doi:10.1093/nar/gkv007.

Sadier A, Sears KE, Womack M. 2022. Unraveling the heritage of lost traits. J Exp Zool B Mol Dev Evol. 338(1–2):107–118. doi:10.1002/jez.b.23030.

Sawa S, Ito T, Shimura Y, Okada K. 1999. FILAMENTOUS FLOWER controls the formation and development of arabidopsis inflorescences and floral meristems. Plant Cell. 11(1):69–86. doi:10.1105/tpc.11.1.69.

Schneider CA, Rasband WS, Eliceiri KW. 2012. NIH Image to ImageJ: 25 years of image analysis. Nat Methods. 9(7):671–675. doi:10.1038/nmeth.2089.

Schultz EA, Haughn GW. 1991. LEAFY, a Homeotic Gene That Regulates Inflorescence Development in Arabidopsis. Plant Cell. 3(8):771–781. doi:10.1105/tpc.3.8.771.

Shannon S, Meeks-Wagner DR. 1991. A Mutation in the Arabidopsis TFL1 Gene Affects Inflorescence Meristem Development. Plant Cell. 3(9):877–892. doi:10.1105/tpc.3.9.877.

Siegfried KR, Eshed Y, Baum SF, Otsuga D, Drews GN, Bowman JL. 1999. Members of the YABBY

gene family specify abaxial cell fate in Arabidopsis. Development. 126(18):4117–4128. doi:10.1242/dev.126.18.4117.

Simon M, Loudet O, Durand S, Bérard A, Brunel D, Sennesal F-X, Durand-Tardif M, Pelletier G, Camilleri C. 2008. Quantitative trait loci mapping in five new large recombinant inbred line populations of Arabidopsis thaliana genotyped with consensus single-nucleotide polymorphism markers. Genetics. 178(4):2253–2264. doi:10.1534/genetics.107.083899.

Siriwardana NS, Lamb RS. 2012. The poetry of reproduction: the role of LEAFY in Arabidopsis thaliana flower formation. Int J Dev Biol. 56(4):207–221. doi:10.1387/ijdb.113450ns.

Smyth DR, Bowman JL, Meyerowitz EM. 1990. Early flower development in Arabidopsis. Plant Cell. 2(8):755–767. doi:10.1105/tpc.2.8.755.

Takagi H, Abe A, Yoshida K, Kosugi S, Natsume S, Mitsuoka C, Uemura A, Utsushi H, Tamiru M, Takuno S, et al. 2013. QTL-seq: rapid mapping of quantitative trait loci in rice by whole genome resequencing of DNA from two bulked populations. Plant J. 74(1):174–183. doi:10.1111/tpj.12105.

Tian T, Liu Y, Yan H, You Q, Yi X, Du Z, Xu W, Su Z. 2017. agriGO v2.0: a GO analysis toolkit for the agricultural community, 2017 update. Nucleic Acids Res. 45(W1):W122–W129. doi:10.1093/nar/gkx382.

Tsukaya H, Byrne ME, Horiguchi G, Sugiyama M, Van Lijsebettens M, Lenhard M. 2013. How do “housekeeping” genes control organogenesis?--Unexpected new findings on the role of housekeeping genes in cell and organ differentiation. J Plant Res. 126(1):3–15. doi:10.1007/s10265-012-0518-2.

Wang Hai, Wang Haiyang. 2015. The miR156/SPL Module, a Regulatory Hub and Versatile Toolbox, Gears up Crops for Enhanced Agronomic Traits. Mol Plant. 8(5):677–688. doi:10.1016/j.molp.2015.01.008.

Wang L, Ming L, Liao K, Xia C, Sun S, Chang Y, Wang H, Fu D, Xu C, Wang Z, et al. 2021. Bract suppression regulated by the miR156/529-SPLs-NL1-PLA1 module is required for the transition from vegetative to reproductive branching in rice. Mol Plant. 14(7):1168–1184. doi:10.1016/j.molp.2021.04.013.

Wang L, Yin H, Qian Q, Yang J, Huang C, Hu X, Luo D. 2009. NECK LEAF 1, a GATA type

1076 transcription factor, modulates organogenesis by regulating the expression of multiple
1077 regulatory genes during reproductive development in rice. Cell Res. 19(5):598–611.
1078 doi:10.1038/cr.2009.36.
1079 Weigel D. 1995. The genetics of flower development: from floral induction to ovule
1080 morphogenesis. Annu Rev Genet. 29:19–39. doi:10.1146/annurev.ge.29.120195.000315.
1081 Weigel D, Alvarez J, Smyth DR, Yanofsky MF, Meyerowitz EM. 1992. LEAFY controls floral
1082 meristem identity in Arabidopsis. Cell. 69(5):843–859. doi:10.1016/0092-
1083 8674(92)90295-n.
1084 Whipple CJ. 2017. Grass inflorescence architecture and evolution: the origin of novel signaling
1085 centers. New Phytol. 216(2):367–372. doi:10.1111/nph.14538.
1086 Whipple CJ, Hall DH, DeBlasio S, Taguchi-Shiobara F, Schmidt RJ, Jackson DP. 2010. A conserved
1087 mechanism of bract suppression in the grass family. Plant Cell. 22(3):565–578.
1088 doi:10.1105/tpc.109.073536.
1089 Wickham H. 2007. Reshaping Data with the reshape Package. Journal of Statistical Software.
1090 21(12):1–20.
1091 Wickham H. 2016. ggplot2: Elegant Graphics for Data Analysis. Springer-Verlag New York.
1092 https://ggplot2.tidyverse.org.
1093 Wickham H, François R, Henry L, Müller K, Vaughan D. 2023. dplyr: A Grammar of Data
1094 Manipulation. https://dplyr.tidyverse.org.
1095 Wickham H, Vaughan D, Girlich M. 2024. tidyr: Tidy Messy Data. https://tidyr.tidyverse.org.
1096 Wu G, Poethig RS. 2006. Temporal regulation of shoot development in Arabidopsis thaliana by
1097 miR156 and its target SPL3. Development. 133(18):3539–3547. doi:10.1242/dev.02521.
1098 Wu T, Hu E, Xu S, Chen M, Guo P, Dai Z, Feng T, Zhou L, Tang W, Zhan L, et al. 2021.
1099 clusterProfiler 4.0: A universal enrichment tool for interpreting omics data. The
1100 Innovation. 2(3):100141. doi:10.1016/j.xinn.2021.100141.
1101 Xiao Y, Guo J, Dong Z, Richardson A, Patterson E, Mangrum S, Bybee S, Bertolini E, Bartlett M,
1102 Chuck G, et al. 2022. Boundary domain genes were recruited to suppress bract growth
1103 and promote branching in maize. Sci Adv. 8(24):eabm6835.
1104 doi:10.1126/sciadv.abm6835.

Xu M, Hu T, McKim SM, Murmu J, Haughn GW, Hepworth SR. 2010. Arabidopsis BLADE-ON-PETIOLE1 and 2 promote floral meristem fate and determinacy in a previously undefined pathway targeting APETALA1 and AGAMOUS-LIKE24. Plant J. 63(6):974–989. doi:10.1111/j.1365-313X.2010.04299.x.

Xu Y-C, Niu X-M, Li X-X, He W, Chen J-F, Zou Y-P, Wu Q, Zhang YE, Busch W, Guo Y-L. 2019. Adaptation and Phenotypic Diversification in Arabidopsis through Loss-of-Function Mutations in Protein-Coding Genes[OPEN]. Plant Cell. 31(5):1012–1025. doi:10.1105/tpc.18.00791.

Zhao Y, Medrano L, Ohashi K, Fletcher JC, Yu H, Sakai H, Meyerowitz EM. 2004. HANABA TARANU is a GATA transcription factor that regulates shoot apical meristem and flower development in Arabidopsis. Plant Cell. 16(10):2586–2600. doi:10.1105/tpc.104.024869.

Supporting Information

Figures S1 to S16

Figure S1: Basal bracts are common among *Brassicaceæ* tribes and their presence is not correlated to broad geographic nor genetic origin in *A. thaliana.*

Figure S2: Comparing basal bract formation in *Tsu-0* with bracts forming in a bract-making sister species.

Figure S3: Known bract mutants in *A. thaliana* display abnormal floral phenotypes and indeterminacy.

Figure S4: Bracts of mutants impaired in floral meristem identity genes are not located at the floral transition like *Tsu-0* natural basal bracts.

Figure S5: Known bract mutants in *A. thaliana* do not display bracts specifically at the floral transition.

Figure S6: Plastochron variation and flowering heterochronies in *Tsu-0* versus *Col-0* accessions

Figure S7: Bulk segregant analysis of basal bract formation (*Tsu-0* x *Col-0*) identifies four putative QTLs.

Figure S8: Quantitative genetics of basal bracts formation in *Tsu-0* using a set of RILs with the reference accession *Col-0*.

Figure S9: Finer mapping of QTLs.

Figure S10: QTL1b* identified for basal bract correlates with a higher cauline branch number.

Figure S11: Transgressive phenotypes in RILs and their genetic determinism provide further information of the genetic pathways involved.

Figure S12: Transcriptomic profile associated with basal bract formation

Figure S13: Transcriptomic cross-comparisons between bract mutants and *Tsu-0* at T stage capture an enrichment for processes related to photosynthesis and provide a short list of 33 causal candidate genes.

Figure S14: GO term analysis at T stage and the identification of anthocyanin biosynthesis and SA-responding pathway enrichment among putative bract regulators.

Figure S15: Temporal Registration of expression dynamics in *Tsu-0* over the floral transition for genes related to bract development, floral identity and floral transition.

Figure S16: A working model for natural basal bract formation in *Arabidopsis thaliana.*

Tables S1 to S8 are large spreadsheets available for download:

Table S1: List of annotated genes lying in mapped QTLs controlling bracts in *Tsu-0*, with additional information from RNAseq and genomic variant analysis.

Table S2: Intersection of genes differentially expressed in *Tsu-0* at stage T and specifically in the *jagged-5D* mutant meristem and mapped within Tsu-0 bract QTLs.

Table S3: Putative bract regulators in *Tsu-0* identified by clustering apart expression from bract and non-bract making stages.

Table S4: Details for all genes associated with “response to salicylic acid” about their expression at stage in *Tsu-0* and their identification as putative bract regulators.

Table S5: Details for all genes associated with anthocyanin metabolism about their expression at stage in *Tsu-0* and their identification as putative bract regulators.

Table S6: Genotypes of all RIL and HIF lines used in this study.

Table S7: SNP information relative to new KASP genotyping markers used in this study.

Table S8: SNP information relative to new sanger genotyping markers used in this study and associated primers.

Figure legends

Figure 1: **The presence of basal bracts is a common, natural trait in *Arabidopsis thaliana* with quantitative variations among genetic backgrounds**. **A**, Examples of bracts (red

arrows) in different angiosperms. *Brassicaceae* are mostly bractless but some species retain bracts at the base of inflorescence branches (e.g. in *L. maritima*). In *A. thaliana*, some natural accessions display basal bracts (e.g. *Tsu-0*) while others do not (e.g. *Col-0*). Schematic phylogenetic relationships are indicated with a cladogram below the pictures. White stars: first ebracteate flowers following previous bracteate flowers **B**, (from left to right) *A. thaliana*'s basal bracts can be true leaves or just small rudimentary filamentous structures at the base of the floral pedicel (red arrows). These structures are absent in younger flowers, as in the reference *Col-0* accession (rightmost panel, black arrowhead). **C**, Details of basal bracts by scanning electron microscopy in a *Tsu-0* inflorescence tip (left panel), showing a bract on the first flower (red arrow) and swollen base of pedicels on the two following flowers (red arrowhead). Right panel: pedicels of *Col-0* plants do not show such structures (black arrowhead). **D**, Occurrence of basal bracts in different accessions, assessed by the percentage of plants with at least one basal bract in the inflorescence. Each dot is the average value of several plants (number indicated by dot size) of a scoring assay. A box plot indicates several assays per line and thicker horizontal black lines are the median value of all scoring assays (range 1-3) in the accession. *Col-0* and *Tsu* are highlighted in green and red, respectively. The geographical origin of each strain is located in the world map below. **E**, Definition of a quantitative bract score for a single plant (see main text for detail). **G**, Quantification of basal bracts in different accessions using the bract score.

Figure 2: **Flowers bearing bracts express high levels of LFY and do not display mutant phenotypes**

A, B. Confocal live imaging of the main meristems of *Col-0* (**A**) and *Tsu-0* (**B**) plants at floral transition, expressing a pLFY transcriptional reporter (magenta) and a membrane marker (green) for morphology (top-view projections of stack acquisitions). Green arrowheads: branches, ordered with decreasing numbers from the floral transition; white arrows: flowers ordered with increasing numbers from the floral transition. In both genotypes, pLFY expression is absent from branch meristems and suddenly appears in the first flower onwards. Representative pictures of at least 6 plants per genotype captured at floral transition.

C, side-view of the first flower from image B (*Tsu-0*): a bract (red arrow) is visible on the abaxial side of this young flower.

D, Number of floral organs in flowers with (dark red) or without (light red) bract in *Tsu-0* plants.

E, F. Side views by confocal live imaging of *Tsu-0* flowers with bracts (red arrow) expressing the pLFY reporter (magenta) and the green morphological marker. Flowers show two

developmental stages older than C and with increasing age from E to F, as shown by the growing abaxial sepal on top of the flower. pLFY is expressed at low levels in the bract margins (magenta arrow).
Scale bars: 50 µm

Figure 3: **Variation in natural basal bract frequency is not correlated with branch position, plastochron length or light conditions, but with variation in flowering time**
A, Correlation study between the number of lateral (cauline) branches and the number of bracts on the main stem only in *Col-0* and *Tsu-0* plants (green and red, respectively). (Pearson test, p-value > 0.1).
B, Effect of different light regimes on bract scores in *Col-0* and *Tsu-0* plants (green and red, respectively). LD and SD stand for long- and short-day conditions, respectively and CL stands for continuous light (see methods). Numbers (e.g. 20SD > LD) indicate the number of days in the first condition before transfer to the second. The number of plants scored is indicated below each bar.
C, Cumulated production of organs over time for *Col-0* and *Tsu-0* plants counted in microdissected shoot apices (green and red, respectively, each time point averaging 5 to 10 plants): the time window when plants make the floral transition is indicated by a horizontal arrow and vertical dashed lines. The rate of organ production (inverse to the plastochron) in this period is computed from the local slope of the curve. Plants were cultured for 21 days in short-day conditions before transfer in long-day (LD) conditions (see methods).
D, Result of three independent experiments of plastochron measurements at flowering transition (see also fig. S5).
E, Differences in flowering time between *Col-0* and *Tsu-0* accession measured as bolting time in days (left) or as the number of vegetative nodes (rosette leaves and cauline leaves/branches) before the first flower on the main stem. Plants grown in LD conditions, N = 58 plants per genotype in two independent replicates.
F, Correlation study between the bract score and the flowering time (assayed when the first flower opens) in different accessions, labelled with different colours. Each dot is a plant and a linear regression standard deviation is computed for each accession.

Figure 4: **Identification of 4 major QTLs controlling basal bract formation in *Tsu-0* suggests unknown genetic pathways**. **A**, Genetic transmission of bract score in F1 and F2 hybrids from a cross between *Col-0* and *Tsu-0* parent plants. **B**, QTL mapping for bract score in

a set of RILs identifies four putative QTLs, two in chromosome 1 (1a and 1b) and two in chromosome 5 (5a and 5b). Dotted horizontal red lines indicate three different significance thresholds computed from 2000 permutations. On top of the graph, H^2 indicates the (broad-sense) heritability of the bract score computed among the RIL set. **C**, Genotype of the F6 generation of the line RIL334 in chromosome 1, showing a heterozygotic region overlapping with QTL1a. **D**, Chromosome 1 genotypes of selected lines forming a heterologous inbred family (HIF) obtained from RIL334 after two more generations of selfing (F8). **E**, Box plots of bract scores of the different lines from the "334 family" (blue boxes) with parental controls (*Col-0*: green, *Tsu-0*: red, N > 20 plants per line). Segregating bract scores within the family map a narrower region, QTL1a*, spanning 541 annotated genes. **F**, Genotype of the F6 generation of the line RIL488 in chromosome 1, showing a heterozygotic region overlapping with QTL1b. **G**, Chromosome 1 genotypes of selected HIF lines obtained from RIL488 at F8 and (**H**) a box plot of their bract scores (blue boxes), with parental controls (*Col-0*: green, *Tsu-0*: red, N > 21 plants per line). This maps a narrower region, QTL1b*, spanning 332 annotated genes. In E and H, lines not sharing the same letter(s) are statistically different (posthoc Tukey analysis with 0.05 sign. level from a glm of bract scores fitted with a quasi-poisson distribution). **I**, Final genetic mapping of the 'basal bract' trait in *Tsu-0* and the location of genes reported to impact bract development in previous mutant studies.

Figure 5: **Transcriptomic divergence between *Tsu-0* and *Col-0* meristems peaks at the floral transition and suggests an unknown developmental control for natural basal bract formation**

A, Scanning electron microscopy showing the evolution of the main meristem in both *Col-0* and *Tsu-0* at the four different stages (V, L, T, F) used for RNAseq. Plants were first synchronized by 21 days of a non-inductive short-day light regime before a transfer to inductive long days. The date after the transfer is indicated in the top-right corner of each picture. Green arrowheads point to branches (with a leaf) while magenta arrowheads point to the first flowers produced after floral transition. In *Tsu-0*, red arrows show bracts.

B, Dynamics of the expression levels of FT, LFY and AP1 (three important regulators of floral transition and identity) in both *Col-0* (green) and *Tsu-0* (red) over the four developmental stages. Differential expression analysis reveals no difference at any stage between the two accessions.

C, Bar plots of the number of genes differentially expressed between two consecutive stages in *Col-0* (green) and *Tsu-0* (red). The number of changes peaks at the V-to-T stage transition,

especially in *Tsu-0*.

D, Bar plots of the number of differentially expressed genes (DEG) between *Col-0* and *Tsu-0* at each stage of the time course. T stage is when the highest number of DEG is measured (on top of the bar, different letters indicate the statistical difference with a chi-square test of homogeneity after posthoc analysis).

E, Dynamics of the expression levels of three previously known "bract" genes, showing a significant difference at least at the T stage between *Col-0* (green) and *Tsu-0* (red). Two stars mean that the genes are differentially expressed and the fold change is superior to 1.

G, Strategy to cluster genes based on the presence/absence of leaf and/or bract in the different combinations of stages and genotypes (see text for details).

H, Volcano plot of gene expressions at the T stage between the two accessions. All genes expressed in the SAM are plotted (n=21,652 grey dots) but only the genes fulfilling the clustering condition defined in G ("putative bract regulators") are highlighted in orange and blue for up- and down-regulation, respectively (n=124). Vertical dashed lines: absolute fold change superior to 1, horizontal dashed line: significance threshold at 5.10^{-2} (adjusted p.value with fdr method).

I, Representative pictures of micro-dissected meristems in *Col-0* (upper row) and *Tsu-0* (lower row) just at or before (left) or after (middle) stage T (N>15 for each genotype) and a close-up of the base of the bolted main stem (right). At stage T, *Tsu-0* meristems display a typical anthocyanin red coloration just below the meristem, which is not observed in *Col-0*. After bolting, both genotypes show anthocyanin coloration at the base of the stem. Scale bars: 100 µm (left and middle), 1 cm (right).

J, Examples of the expression profile of two candidate genes, showing an up- (left) and a down- (right) regulation at the T stage. *DFR* is an enzyme involved in anthocyanin biosynthesis while *FMOGS-OX7* is annotated as a salicylic acid responding enzyme. Two stars mean that the genes are differentially expressed and the fold change is superior to 1. The bract and bract-less clusters are outlined with a solid and dashed circle, respectively, while the horizontal dotted line highlights their separation.

Figure 6: **Massive and complex transcriptional desynchronisation coexist in *Tsu-0* across the floral transition.**

A, PCA of RNAseq data from microdissected meristems of *Col-0* and *Tsu-0* over the four sampled stages (biological replicates averaged per time points). The two main axes of the PCA can be interpreted as developmental time and genotype, respectively.

B, Examples of temporal registration of gene dynamics (right panels) between *Col-0* (green) and *Tsu-0* (red) from scaled expression levels (left panel). Dots represent the expression levels of independent biological replicates, while lines indicate the mean expression level at each time point. In the right panel, the green (or red) dotted curves represent the fitted models for *Col-0* (or *Tsu-0*) independently, while the grey dotted curve represents the joint model for both *Col-0* and *Tsu-0*. If the green and red dotted curves are used, it means the two time series are best explained by two independent models, indicating they are not similar. Conversely, if the grey dotted curve is used, it suggests that a single model best explains both time series, indicating they are similar. The name of the gene plotted is indicated on the left of each row. These four genes exemplify the four possible categories (from top to bottom, respectively): genes that cannot be registered (N = 43, *e.g. CYP705A9*), genes with identical temporal dynamics (shift = 0, *e.g. AP1,* see also Fig. 5B) and genes whose expression dynamics in *Tsu-0* must be shifted negatively (*e.g. DFR,* see also Fig. 5J) or positively (*e.g*. *AG*) to align with *Col-0*. The last column provides a biological interpretation of the computed shift (see main text): a null shift indicates that the expression dynamics in *Tsu-0* stay "*in phase*" with floral transition while negative or positive shifts indicate that the expression dynamics in *Tsu-0* are desynchronized later or earlier, respectively, than the phenotypic progression of floral transition.

C, Distribution of heterochronic shifts between *Tsu-0* and *Col-0* on the entire meristematic transcriptome, computed by the registration method from B. The shift value is colour-coded in a red-to-blue gradient from -1 to 1.

D, GO term enrichment analysis associated with the three categories of heterochronic shifts. The list of all significant 'biological process' GO terms (BH-adjusted p.value < 0.05) was simplified using semantic similarity (cutoff = 0.7) and the Rich Factor was computed for the remaining terms, revealing the proportion of genes involved among all the genes associated with this GO term. Dot size indicates the count of genes and the color scale is the statistical significance (BH-adjusted p.value) of the enrichment in the shift category. Stars indicate GO terms referring to developmental processes.